Developmental Biology 356 (2011) 383–397

Contents lists available at ScienceDirect

Developmental Biology

journal homepage: www.elsevier.com/developmentalbiology

Genomes and Developmental Control

Redundant and dosage sensitive requirements for *Fgf3* and *Fgf10* in cardiovascular development

Lisa D. Urness [a], Steven B. Bleyl [b,c], Tracy J. Wright [a], Anne M. Moon [a,c,d], Suzanne L. Mansour [a,c,*]

[a] Department of Human Genetics, University of Utah, Salt Lake City, UT 84112, USA
[b] Department of Pediatrics, University of Utah School of Medicine, Salt Lake City, UT 84132, USA
[c] Department of Neurobiology and Anatomy, University of Utah, Salt Lake City, UT 84132, USA
[d] Molecular Medicine Program, University of Utah, Salt Lake City, UT 84112, USA

ARTICLE INFO

Article history:
Received for publication 6 December 2010
Revised 6 May 2011
Accepted 20 May 2011
Available online 12 June 2011

Keywords:
FGF signaling
Cardiovascular development
Mouse genetics

ABSTRACT

Heart development requires contributions from, and coordinated signaling interactions between, several cell populations, including splanchnic and pharyngeal mesoderm, postotic neural crest and the proepicardium. Here we report that *Fgf3* and *Fgf10*, which are expressed dynamically in and near these cardiovascular progenitors, have redundant and dosage sensitive requirements in multiple aspects of early murine cardiovascular development. Embryos with $Fgf3^{-/+};Fgf10^{-/-}$, $Fgf3^{-/-};Fgf10^{-/+}$ and $Fgf3^{-/-};Fgf10^{-/-}$ genotypes formed an allelic series of increasing severity with respect to embryonic survival, with double mutants dead by E11.5. Morphologic analysis of embryos with three mutant alleles at E11.5–E13.5 and double mutants at E9.5–E11.0 revealed multiple cardiovascular defects affecting the outflow tract, ventricular septum, atrioventricular cushions, ventricular myocardium, dorsal mesenchymal protrusion, pulmonary arteries, epicardium and fourth pharyngeal arch artery. Assessment of molecular markers in E8.0–E10.5 double mutants revealed abnormalities in each progenitor population, and suggests that *Fgf3* and *Fgf10* are not required for specification of cardiovascular progenitors, but rather for their normal developmental coordination. These results imply that coding or regulatory mutations in *FGF3* or *FGF10* could contribute to human congenital heart defects.

Introduction

Development of the heart and great vessels requires a highly choreographed interplay of multipotent progenitor cell populations. Interference with the progenitors, or with their intercellular interactions, leads to congenital heart defects (CHDs), which affect nearly 1% of live births (Bruneau, 2008). The primitive heart tube forms by ventral fusion of dorsally connected, bilaterally situated wings of splanchnic mesoderm referred to as the first heart field (FHF). These cells contribute most of the myocardium and endocardium of the primitive left ventricle, and a small proportion of the cells in the right ventricle and atria. Subsequent addition of a second mesodermal cell population, located dorsal and medial to the FHF, and termed the second heart field (SHF), lengthens the heart tube from both the anterior (outflow, or arterial) and posterior (inflow or venous) poles. The SHF is the major contributor of myocardium and endocardium to the outflow tract (OFT), the right ventricle, and dorsal mesenchymal protrusion (DMP), as well as to a majority of the atria and a portion of the inflow tract (IFT) (Abu-Issa and Kirby, 2007; Chien et al., 2008; Snarr et al., 2008). Developmental abnormalities of these mesodermal cells can lead to a variety of cardiac defects, depending on the timing of perturbation. Early perturbations can disrupt heart tube looping, ventricular growth or myocardial cell differentiation. Dysfunction of the SHF causes a spectrum of cardiac malformations affecting the arterial pole and OFT, including tetralogy of Fallot, double outlet right ventricle and persistent truncus arteriosus (PTA) (Moon, 2008; Vincent and Buckingham, 2010; Ward et al., 2005). SHF defects also cause malformations of the IFT, including atrioventricular (AV) septal and sinus venosus defects, as well as anomalous pulmonary venous return (Bleyl et al., 2010; Goddeeris et al., 2008; Mommersteeg et al., 2010).

Higher vertebrate OFT development depends not only on cells contributed by the SHF, but also on the cardiac neural crest (CNC), which originates from the dorsal hindbrain, posterior to the otic vesicle (rhombomeres (r)6–8). CNC cells undergo an epithelial-to-mesenchymal transition (EMT), and then migrate ventrally through pharyngeal arches 3, 4 and 6, and into the OFT. CNC contributes relatively few cells to the mature heart proper—the CNC lineage is found mainly in the smooth muscle of the great arteries, the aorticopulmonary septum and the cardiac ganglia. However, CNC interactions with the SHF and its derivatives play critical roles in cardiovascular development, supporting the deployment of SHF cells

* Corresponding author at: Department of Human Genetics, University of Utah, 15 N 2030 E RM 2100, Salt Lake City, UT 84112-5330, USA. Fax: +1 801 581 7796.
E-mail address: suzi.mansour@genetics.utah.edu (S.L. Mansour).

0012-1606/$ – see front matter © 2011 Elsevier Inc. All rights reserved.
doi:10.1016/j.ydbio.2011.05.671

to the growing OFT, and subsequent OFT septation. Defects in CNC development can cause the same spectrum of defects as seen with abnormal SHF function (Bruneau, 2008; Kirby and Hutson, 2010; Snider et al., 2007).

Another source of cardiac cells is the proepicardial organ (PEO), which forms in the mesothelium just posterior to the developing heart, at the anterior surface of the septum transversum. Proepicardial cells migrate over the surface of the heart, forming the epicardium; a thin layer of cells covering the heart. Some epicardial cells undergo an EMT, enter the heart proper, and generate the smooth muscle of the coronary vasculature and the heart fibroblasts. The epicardium also provides signals supporting ventricular myocardial growth (Carmona et al., 2010; Gittenberger-de Groot et al., 2010; Ratajska et al., 2008). Whether the PEO comprises a subpopulation of the SHF or is a completely independent contributor is unclear. The latest lineage tracing data suggest that the proepicardium and SHF myocardial contributors to the IFT have a common origin (van Wijk et al., 2009). Thus, defects occurring in the epicardial lineage, after separation from the posterior SHF, affect the developing coronary vasculature and induction of the ventricular compact myocardium and interstitial fibroblast network. Defects arising prior to the lineage separation, may affect both the IFT and the epicardium (Mommersteeg et al., 2010).

Fibroblast Growth Factors (FGFs) are among the critical signals controlling communication within and between developing heart progenitors. The secreted FGFs comprise an 18-member ligand family that signals through seven major receptor tyrosine kinase isoforms encoded by four genes (Itoh and Ornitz, 2008). FGF8 is the best understood of these signals regulating cardiovascular development. Very early expression of *Fgf8*, presumably in the vicinity of the node, controls left–right axis formation, and thus normal looping of the heart tube (Meyers and Martin, 1999). Later expression of *Fgf8* in the SHF mesoderm is required for expansion of the anterior heart tube and normal OFT alignment (Brown et al., 2004; Ilagan et al., 2006; Park et al., 2006). Expression in the pharyngeal ectoderm is required for normal aortic arch artery development (Macatee et al., 2003; Park et al., 2006). Although ablation of *Fgf8* from the pharyngeal endoderm alone does not disrupt OFT development, combined *Fgf8* ablation from endoderm and the SHF causes PTA in 100% of mutants (Park et al., 2006), phenocopying CNC ablation in chick (Kirby et al., 1985). However, the effects of FGF8 on neural crest are likely indirect, as conditional neural crest-specific deletion of *Fgfr1* and *Fgfr2*, or indeed the FGF downstream signaling pathway coordinated by *Frs2α*, has no effect on heart development (Park et al., 2008; Zhang et al., 2008).

Fgf15 is also required for normal OFT alignment and for ventricular septation (Vincentz et al., 2005). Defective CNC invasion of the OFT cushions in *Fgf15* null embryos is proposed as the mechanism underlying the mutant phenotypes, but the relationship between these defects and the function of FGF15, derived from the pharyngeal endoderm, ectoderm, and neurectoderm adjacent to the developing neural crest (Vincentz et al., 2005; Wright et al., 2004), has not yet been investigated.

Fgf10, which is expressed prominently in the SHF (Kelly et al., 2001), does not by itself have a major function in heart development. *Fgf10* null embryos, which die at birth due to lung aplasia, also lack pulmonary arteries and veins and have hearts with a slightly abnormal position within the thoracic cavity (Marguerie et al., 2006). However, *Fgf10* is strongly implicated in heart development because it interacts genetically with *Fgf8*. The penetrance of pharyngeal arch artery 4 (PAA4) and OFT defects is increased in FHF/SHF conditional *Fgf8* mutants by removal of *Fgf10* alleles (Watanabe et al., 2010). Furthermore, ablation of the major FGF10 receptor, FGFR2b, causes more severe heart abnormalities than ablation of *Fgf10*, including ventricular septal defect (VSD) and delayed OFT septation, leading to alignment defects, and thin and poorly trabeculated ventricles (Marguerie et al., 2006). This suggests that other FGFR2b ligands (i.e. FGF3, FGF7, or FGF22) might be functionally redundant with FGF10 for some aspects of cardiovascular development.

Here we report that *Fgf3* and *Fgf10* have redundant and dosage sensitive requirements in multiple aspects of early cardiovascular development. Embryos with $Fgf3^{-/+}$;$Fgf10^{-/-}$, $Fgf3^{-/-}$;$Fgf10^{-/+}$ and $Fgf3^{-/-}$;$Fgf10^{-/-}$ genotypes formed an allelic series of increasing severity with respect to embryonic survival, with double mutants dead by E11.5. Morphologic analysis of triple-allelic mutants ($Fgf3^{-/+}$; $Fgf10^{-/-}$ and $Fgf3^{-/-}$;$Fgf10^{-/+}$) at E11.5–E13.5 and double mutants ($Fgf3^{-/-}$;$Fgf10^{-/-}$) at E9.5–E11.0 revealed multiple cardiovascular defects affecting the OFT, ventricular septum, AV cushions, ventricular myocardium, DMP, pulmonary arteries, epicardium and PAA4. Molecular marker studies of double mutants revealed abnormalities in each cardiac progenitor cell population. There were reduced streams of postotic neural crest and strikingly, expression of *Isl1*, encoding a critical SHF transcription factor, was transiently decreased in the double mutant SHF at E8.5, whereas *Nkx2-5* expression in cardiomyocytes was not affected until E10.5, and *Fgf8* and *Fgf15* were never affected. In addition, epicardial markers were reduced in double mutants by E10.5. We propose that the double mutant cardiovascular defects are caused by loss of redundant, dosage sensitive FGF3 and FGF10 signals that act directly on the SHF and its derivatives, and indirectly on the CNC to coordinate their development. In addition, our results support a very early role for these FGFs in epicardial/myocardial interactions. Finally, we suggest *FGF3* and *FGF10* as candidate genes contributing to human CHDs.

Materials and methods

Mutant mice and genotyping

All mouse studies complied with protocols approved by the University of Utah Institutional Animal Care and Use Committee. The original double heterozygous intercross involving $Fgf3^{neo}$ ($Fgf3^{tm1Mrc}$; MGI:1931059) and $Fgf10^{neo}$ ($Fgf10^{tm1Wss}$; MGI:1927833) null alleles and their genotyping were described in Wright and Mansour (2003). The newer *Fgf3* and *Fgf10* conditional ($Fgf3^{tm1.2Sms}$; MGI:4456396 and $Fgf10^{tm1.2Sms}$; MGI:4456398, each abbreviated "c") and null alleles ($Fgf3^{tm1.1Sms}$; MGI:3767558 and $Fgf10^{tm1.1Sms}$; MGI:3526181; each abbreviated "*Δ2*" or "–"), the $Hprt^{Cre}$ allele ($Hprt^{tm1(cre)Mnn}$; MGI:2181632), and genotyping protocols used in this study are described in Urness et al. (2010). All progenitors used in crosses came from a mixed genetic background primarily comprised of C57Bl/6 and various 129 "S" and "P" substrains. Embryos were considered to be E0.5 at noon on the day of mating plug detection.

Histology and three-dimensional reconstructions

E9.5 embryos were harvested in cold PBS and incubated in 50 μg/ml of verapamil (Sigma V4629) in phosphate-buffered saline for 5–10 min to relax the myocardium. Embryos were then fixed in 4% paraformaldehyde solution, followed by standard paraffin wax embedding, transverse sectioning at 8 μm and hematoxylin and eosin (H&E) staining. For three-dimensional visualization of E10.5 specimens and standard histologic preparation of E11.5 and E13.5 specimens, embryos were fixed in Bouin's solution prior to wax embedding. Transverse 8 μm sections were cut from the anterior end of the pharyngeal arches to the ductus venosus and stained with H&E. E10.5 serial stained sections were digitally imaged at 10× magnification. Images were aligned, segmented and reconstructed using the Amira software package version 5.0 (Visage Imaging, Inc., San Diego).

Immunohistochemistry and intravascular dye injection

Tuj1 immunohistochemistry (directed against neuronal class III ß-tubulin) was performed according to Chisaka et al. (1992). Vascular

patency was assessed by microinjection of India ink (Pelican) into the common ventricle of E10.5 embryos harvested in PBS (yolk sacs reflected, but not removed). The embryos were placed in Carnoy's fixative and photographed immediately following injection.

In situ hybridization

Whole-mount non-radioactive in situ hybridization of embryos, post-fixation, cryoprotection and sectioning at 14 μm was performed as described previously (Urness et al., 2010). Control and double mutant embryos were developmentally matched to within 2 somites and hybridized and developed in the same tubes for the same amount of time. Cloned mouse cDNAs used to prepare digoxigenin-labeled RNA probes included *Fgf3* and *Fgf10* (Wright and Mansour, 2003), *Fgf15* (Wright et al., 2004), *Fgf8* (Ladher et al., 2005), *Isl1* and *Mef2c* (Park et al., 2006), *Wnt1* and *Bmp4* (Hatch et al., 2007), *Sox9* (Urness et al., 2010) and *Tcf21 (Epicardin*; GenBank accession NM_011545, purchased from OpenBiosystems). *Sox10, Tbx1*, *Tdgf1* (*Cripto*) and *Wnt11*, *Pax3*, *Hand2* (*dHand*), *Tbx18*, *Cadh6, Nkx2-5 and Myl7 (Mlc2a)*-containing plasmids for probe preparation were kindly provided by Drs. P. Koopman, B. Morrow, Y. Saijoh, G. Kardon, D. Guns, A. Kispert, O. Chisaka, D. Li and S. Evans, respectively. RNA probes specific for the 3′ UTR of *Gata4* and *Wnt2a* were generated by T7 polymerase-directed transcription of DNA fragments generated by PCR-amplification of genomic DNA using a *Gata4* forward primer, 5′-CAAGGAGGAA-CAAAACCTGCTACC-3′ with a T7 promoter-tagged *Gata4* reverse primer, 5′-ggatcctaatacgactcactatagggagGACAAGGAAGAATCTCTGG-GAGC-3′ and a *Wnt2a* forward primer, 5′-TTTTCCCAGATTCCAA-CAACCC-3′ with a T7 promoter-tagged *Wnt2a* reverse primer, 5′-ggatcctaatacgactcactatagggagCCATTCCCCTTTCAGATTCTCTCC-3′ as described by Urness et al. (2010). Note that the $Fgf10^{\Delta 2}$ transcript, which has a premature termination codon rendering it unable to produce FGF10, is stable (RT-PCR data not shown) and can be detected in $Fgf10^{\Delta 2/\Delta 2}$ mutant embryos by in situ hybridization using our standard probe.

Results

Fgf3 and Fgf10 are required for viability after E11.0

Our previous studies of *Fgf3* and *Fgf10* in inner ear development revealed that although $Fgf3^{-/-}$ or $Fgf10^{-/-}$ mutant embryos were recovered alive and in the expected numbers through E18.5, live $Fgf3^{-/-}$;$Fgf10^{-/-}$ embryos (*Fgf3*/*Fgf10* double null mutants) were not observed after E10.5 (Hatch et al., 2007; Mansour et al., 1993; Wright and Mansour, 2003; T.J.W., L.D.U. and S.L.M., unpublished observations). To assess potential redundant roles for *Fgf3* and *Fgf10* in viability, we intercrossed $Fgf3^{-/+}$;$Fgf10^{-/+}$ mice and observed and genotyped offspring between E8.5 and E15.5 (Table 1A). Between E8.5 and E11.0, embryos of all possible genotypes were found alive in the expected numbers. Of 267 embryos collected between E11.5 and E15.5, all 8 $Fgf3^{-/-}$;$Fgf10^{-/-}$ individuals (~50% of expected number) were dead and resorbing. The recovery of embryos carrying a total of three null alleles was reduced to ~67% of expected, but all other genotypes were recovered at or above the expected number. The few other dead/resorbing embryos were either $Fgf3^{-/-}$ or $Fgf3^{-/-}$;$Fgf10^{-/+}$. To generate double null mutants at a higher frequency, we mated $Fgf3^{\Delta 2/+}$;$Fgf10^{\Delta 2/+}$;$Hprt^{Cre/+}$ females with $Fgf3^{c/c}$;$Fgf10^{c/c}$ males (double mutants expected at 25% vs. 6.25% from the double heterozygous intercross; Urness et al., 2010). Similar to the double heterozygote intercrosses, live double null mutants of less than 40 somites (~E11.0) could be obtained in the expected numbers; however, double null mutants of greater than 40 somites were not recovered, and $Fgf3^{-/-}$;$Fgf10^{-/+}$ embryos were dead or dying at this stage (Table 1B). These data show that *Fgf3* and *Fgf10* are required for viability past E11.0, and that the requirements for these genes are not equivalent, with *Fgf3* more important for survival than *Fgf10*.

Heart development is sensitive to the dosage of both Fgf3 and Fgf10

Midgestational lethality can result from defective heart development (Conway et al., 2003). To determine whether *Fgf3* and *Fgf10* play

Table 1A
The $Fgf3^{-/-}$;$Fgf10^{-/-}$ genotype is lethal after E11.0. $Fgf3^{neo/+}$;$Fgf10^{neo/+}$ animals were intercrossed (Table 1A) or, more recently, $Fgf3^{\Delta 2/+}$;$Fgf10^{\Delta 2/+}$;$Hprt^{Cre/+}$ females were crossed to $Fgf3^{c/c}$;$Fgf10^{c/c}$ males (Table 1B) and embryos were genotyped at the indicated ages. Both the *neo* and *Δ2* alleles are null and are designated as "–"in the table. The number of embryos of each genotype is indicated together with the expected number in parentheses. All genotypes were recovered in the expected numbers between E8.5–E11.0. Genotypes at E11.5–15.5 did not fit the Mendelian expectation, due to lethality of the double mutant class and reduced viability of $Fgf3^{-/-}$;$Fgf10^{-/+}$ embryos. Many of the embryos included in the E8.5–E11.0 double heterozygote intercross totals shown in Table 1A were previously reported and used in studies of inner ear development (Wright and Mansour, 2003). Genotypes of $Fgf3^{-/+}$;$Fgf10^{-/+}$ intercross offspring.

Age	Total #	$Fgf3^{+/+}$ $Fgf10^{+/+}$	$Fgf3^{-/+}$ $Fgf10^{+/+}$	$Fgf3^{-/-}$ $Fgf10^{+/+}$	$Fgf3^{+/+}$ $Fgf10^{-/+}$	$Fgf3^{-/+}$ $Fgf10^{-/+}$	$Fgf3^{-/-}$ $Fgf10^{-/+}$	$Fgf3^{+/+}$ $Fgf10^{-/-}$	$Fgf3^{-/+}$ $Fgf10^{-/-}$	$Fgf3^{-/-}$ $Fgf10^{-/-}$
E8.5—E11.0	1878	127	237	122	212	485	225	123	245	101
	(exp.)	(117)	(235)	(117)	(235)	(470)	(235)	(117)	(235)	(117)
E11.5–E15.5	267	27	46	14(1*)	37	69	22(2*)	19	25	0(8*)
	(exp.)	(17)	(33)	(17)	(33)	(67)	(33)	(17)	(33)	(17)

Table 1B
The $Fgf3^{-/-}$;$Fgf10^{-/-}$ genotype is lethal after E11.0. $Fgf3^{neo/+}$;$Fgf10^{neo/+}$ animals were intercrossed (Table 1A) or, more recently, $Fgf3^{\Delta 2/+}$;$Fgf10^{\Delta 2/+}$;$Hprt^{Cre/+}$ females were crossed to $Fgf3^{c/c}$;$Fgf10^{c/c}$ males (Table 1B) and embryos were genotyped at the indicated ages. Both the *neo* and *Δ2* alleles are null and are designated as "–"in the table. The number of embryos of each genotype is indicated together with the expected number in parentheses. All genotypes were recovered in the expected numbers between E8.5 and E11.0. Genotypes at E11.5–15.5 did not fit the Mendelian expectation, due to lethality of the double mutant class and reduced viability of $Fgf3^{-/-}$;$Fgf10^{-/+}$ embryos. Many of the embryos included in the E8.5–E11.0 double heterozygote intercross totals shown in Table 1A were previously reported and used in studies of inner ear development (Wright and Mansour, 2003). Genotypes of $Fgf3^{-/+}$;$Fgf10^{-/+}$;$Hprt^{Cre/+}$ × $Fgf3^{c/c}$;$Fgf10^{c/c}$ offspring.

Age	Total #	$Fgf3^{-/+}$ $Fgf10^{-/+}$	$Fgf3^{-/-}$ $Fgf10^{-/+}$	$Fgf3^{-/+}$ $Fgf10^{-/-}$	$Fgf3^{-/-}$ $Fgf10^{-/-}$
<40 somites	814	197	235	178	204
	(exp.)	(203.5)	(203.5)	(203.5)	(203.5)
≥40 somites	24	10	0(5*)	9	0
	(exp.)	(6)	(6)	(6)	(6)

* Dead/necrosing embryos.

combinatorial roles in heart development, we first studied embryos carrying three mutant alleles, as these could be recovered as late as E13.5, a time when many heart defects can be assessed. Examination of H&E-stained transverse sections revealed a number of variably penetrant anomalies in such embryos, affecting the OFT (Fig. 1), as well as the AV septum, ventricular myocardium, epicardium and IFT (Fig. 2).

At E13.5, we found persistent truncus arteriosus (PTA) and right aortic arch (red arrow, Fig. 1C) in one of three *Fgf3*$^{-/-}$;*Fgf10*$^{-/+}$ embryos recovered for histology, but not in any of three *Fgf3*$^{-/+}$;*Fgf10*$^{-/+}$ (control) embryos (Fig. 1A), nor in any of the single null mutant (*Fgf3*$^{-/-}$ or *Fgf10*$^{-/-}$; Figs. 1B and D) or *Fgf3*$^{-/+}$;*Fgf10*$^{-/-}$ (Fig. 1E) mutants examined. The other two *Fgf3*$^{-/-}$;*Fgf10*$^{-/+}$embryos examined at this stage did not exhibit OFT defects and were likely rare "escapers" that can survive later in gestation (Table 1A), or even to birth (T.J.W. and S.L.M., unpublished data). At E12.5, OFT defects were seen in both *Fgf3*$^{-/-}$;*Fgf10*$^{-/+}$ (Fig. 1H) and both *Fgf3*$^{-/+}$;*Fgf10*$^{-/-}$ (Fig. 1J) mutants examined. Embryos carrying three mutant alleles had evidence of failure of rotation and alignment of the septating OFT such that the aorta was completely committed to the right ventricle (Figs. 1H and J) at a stage where there was clearly an LV outflow connecting to the aorta in controls (Figs. 1F, G, and I; black arrows). This would likely result in double outlet right ventricle were the embryos to survive and continue OFT development. At E11.5, the OFT of two of three *Fgf3*$^{-/-}$;*Fgf10*$^{-/+}$ embryos was completely occluded with cells (Fig. 1M; red arrow) relative to embryos of all other genotypes (Figs. 1K, L, N, and O). Since this phenotype is incompatible with further survival, this may explain why OFT occlusion was not observed at E12.5–E13.5. Together, these data reveal a previously unappreciated role for *Fgf3* and *Fgf10* in OFT development, with complete loss of *Fgf3* and 50% reduction of *Fgf10* resulting in more penetrant and severe OFT defects than in the other triple-allelic combination.

Moving posteriorly at E13.5, we found VSDs in both *Fgf3*$^{-/-}$;*Fgf10*$^{-/+}$ and in two of four *Fgf3*$^{-/+}$;*Fgf10*$^{-/-}$ embryos examined (Figs. 2C and E; red arrows). Such defects were not described previously in *Fgf3*$^{-/-}$ or *Fgf10*$^{-/-}$ embryos, however, in this genetic background, we found VSDs in both E13.5 *Fgf3*$^{-/-}$ mutants examined (Fig. 2C, red arrow), but not in control (n = 4) or *Fgf10*$^{-/-}$ embryos (Figs. 2A and D). A VSD was also observed in an *Fgf3*$^{-/-}$ embryo at E14.5 (Suppl. Fig. 1), a time when such defects cannot be attributed to variable development in different genetic backgrounds. VSDs might therefore account for the reduced recovery of *Fgf3*$^{-/-}$ mutants at weaning (Hatch et al., 2007; Mansour et al., 1993). In addition, the E13.5 mid-heart sections (Figs. 2A–E), as well those prepared at E12.5 (Figs. 2F–J), and those illustrating the E11.5 OFT defect (Figs. 1K–O), revealed that *Fgf3*$^{-/-}$;*Fgf10*$^{-/+}$ embryos had thin ventricular walls and decreased trabeculae (Figs. 1M and 2C and H) relative to the other genotypes.

At E12.5, we also found that *Fgf3*$^{-/-}$;*Fgf10*$^{-/+}$ embryos showed a marked detachment of the epicardium from the underlying myocardium (Figs. 2H and M; red arrows). Interestingly, the endocardium was also only loosely associated with the myocardium (Fig. 2M; red caret). Both *Fgf3*$^{-/+}$;*Fgf10*$^{-/-}$ mutants (Figs. 2J and O) examined at this stage also showed a degree of epicardial detachment, though not as extreme as that observed in the *Fgf3*$^{-/-}$;*Fgf10*$^{-/+}$ mutants. In contrast, *Fgf3*$^{-/+}$;*Fgf10*$^{-/+}$ (Figs. 2F and K), *Fgf3*$^{-/-}$ (Figs. 2G and L) and the majority (2/3) of *Fgf10*$^{-/-}$ hearts showed firmly adhered epicardia. However, it was possible to find areas of epicardial detachment in some regions of one of the *Fgf10*$^{-/-}$ embryos (Figs. 2I and N).

Finally, E13.5 mutant embryos also showed both expected and unexpected pulmonary vascular defects. As expected (Marguerie et al., 2006), the pulmonary arteries were absent from both *Fgf10*$^{-/-}$ and *Fgf3*$^{-/+}$;*Fgf10*$^{-/-}$ embryos (Figs. 2S and T). We were surprised to find, however, that *Fgf3*$^{-/-}$;*Fgf10*$^{+/-}$ embryos also lacked pulmonary arteries (Fig. 2R), whereas they developed normally in control and *Fgf3*$^{-/-}$ embryos (Figs. 2P and Q). Also as expected, the lungs failed to form in *Fgf10*$^{-/-}$ and *Fgf3*$^{-/+}$;*Fgf10*$^{-/-}$ embryos (Min et al., 1998; Sekine et al., 1999), but unexpectedly, mildly hypoplastic lungs were also observed in both *Fgf3*$^{-/-}$;*Fgf10*$^{+/-}$ embryos (data not shown).

Taken together, these histologic results show that loss of an *Fgf3* allele from the *Fgf10* null background caused OFT alignment and rotation defects, VSD and moderate epicardial detachment. Loss of an *Fgf10* allele from the *Fgf3* null background also led to OFT alignment and rotation defects and, in one case, PTA. These embryos also showed VSD, thin and poorly trabeculated ventricular walls, severe epicardial detachment, pulmonary artery aplasia and lung hypoplasia. Thus, both *Fgf3* and *Fgf10* play previously unappreciated roles in heart and lung development.

Fgf3/Fgf10 double null mutants display first and second heart field and cardiac neural crest-related defects

To assess heart development in the complete absence of *Fgf3* and *Fgf10*, we examined double null mutants at E10.5–11.0, the oldest stage that could be recovered reliably. As reported previously (Urness et al., 2010; Wright and Mansour, 2003), double mutant embryos lacked limbs and otic vesicles, and had short tails (Figs. 3A–C). In addition, most live E10.5 double mutant embryos appeared slightly smaller than *Fgf3*$^{-/+}$;*Fgf10*$^{-/+}$ littermate control embryos (Figs. 3A and B), but some were much smaller than normal, and showed pericardial effusion and chamber dilation, signs of cardiovascular distress and imminent death (Fig. 3C). By E11.0, relative to *Fgf3*$^{-/+}$;*Fgf10*$^{-/+}$ controls (Fig. 3D), the hearts of freshly dissected double mutants beat very slowly or not at all, had severe blood pooling, and the ventricles were noticeably transparent (Fig. 3E). To avoid potential artifact associated with developmental delay and possible necrosis, all embryos analyzed in detail at this stage had the less severe phenotype (as in Fig. 3B). Younger double mutant embryos were similar in size to double heterozygous littermate controls and could only be distinguished (starting at E9.5) by their limb and inner ear agenesis.

Three-dimensional reconstructions of H&E-stained transverse sections of E10.5 control and double mutant embryos (Figs. 3F–I) revealed that some double mutants had a slightly shortened OFT (Figs. 3F and G; white arrow). Double mutants also exhibited thin, poorly trabeculated ventricles, dilated atria (Figs. 3H and I) and unfused atrioventricular cushions (a/v; Figs. 3H–K); the latter may be secondary to atrial dilation. Examination of the posterior pole of the heart revealed a hypoplastic DMP in double mutants (dmp; Figs. 3L and M). This structure arises from the posterior aspect of the SHF, and contributes to the AV septal complex (Goddeeris et al., 2008; Hoffmann et al., 2009; Snarr et al., 2007a, 2007b). More posterior sections of the same pair of embryos showed marked DMP hypoplasia and failure of the DMP to fuse with the anterior IFT wall, with a persistent connection of the pulmonary vein (PV) to both the left atrium (LA) and sinus venosus (SV) in the double mutant (Figs. 3N and O), analogous to IFT defects seen in a mouse model of human total anomalous pulmonary venous return (TAPVR) (Bleyl et al., 2010).

To determine whether developmental heart defects could be identified well before embryonic demise, control and double mutant embryos harvested in the presence of verapamil to eliminate contraction-state effects were compared at E9.5 (Figs. 3P–S). Transverse sections were taken through the anterior (Figs. 3P and Q) and middle (Figs. 3R and S) of the heart. In contrast to controls, both double mutant embryos examined showed hypoplastic AV cushions (Figs. 3Q and S, large red arrows), thin and poorly trabeculated myocardium (Figs. 3Q and S red carets) and detached endocardium that could be due to poor adhesion or excessive cardiac jelly (Fig. 3Q, small arrow). Transverse sections taken through the OFT of E11.0 embryos (shown in Figs. 3D and E) revealed a hypocellular OFT in the double mutant (Fig. 3U, red arrow) relative to the control littermate (Fig. 3T). Sections taken through the middle of the heart

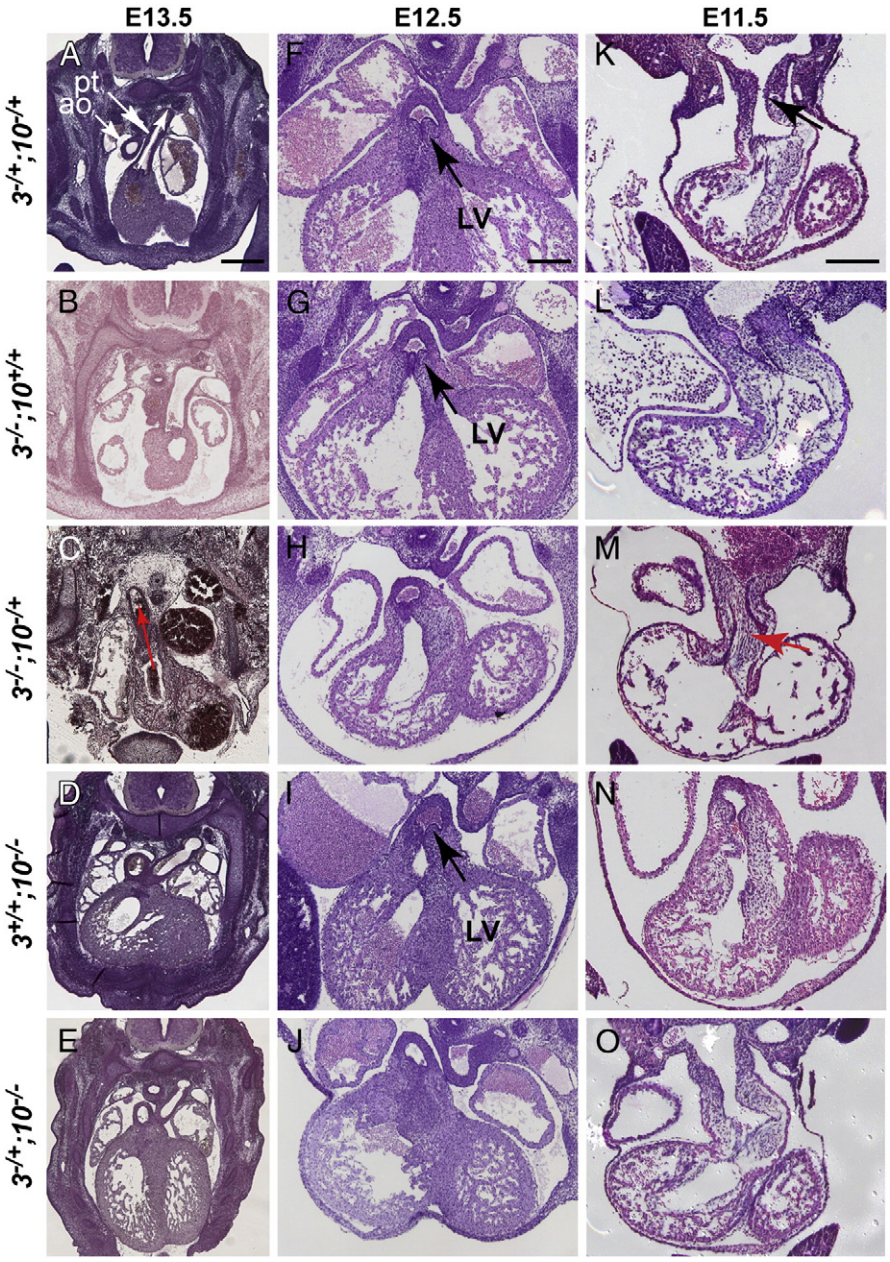

Fig. 1. Embryos carrying both combinations of three *Fgf3* and *Fgf10* null alleles have abnormal OFT development. H&E-stained transverse sections taken through the anterior heart of E11.5–E13.5 embryos. Genotypes are abbreviated to the left of each row (3, *Fgf3*; 10, *Fgf10*). Embryonic age is indicated at the top of each column. (A) E13.5 $Fgf3^{-/+}$;$Fgf10^{-/+}$ (control) embryo demonstrating normal outflow tract (OFT) directionality (white arrow) and septation of the aorta (ao) and pulmonary trunk (pt). Similarly staged $Fgf3^{-/-}$ (B), $Fgf10^{-/-}$ (D), and $Fgf3^{-/+}$;$Fgf10^{-/-}$ (E) embryos also showed normal OFT septation and patterning. (C) $Fgf3^{-/-}$;$Fgf10^{-/+}$ was the only genotype presenting at E13.5 with PTA and a rightward-oriented OFT (red arrow). (F) E12.5 control embryo demonstrating normal communication of the aorta with the left ventricle (LV, black arrows). Aortic OFT development was also normal in E12.5 $Fgf3^{-/-}$ (G), and $Fgf10^{-/-}$ (I) mutants. Both triple allelic mutants, $Fgf3^{-/-}$;$Fgf10^{-/+}$ (H) and $Fgf3^{-/+}$;$Fgf10^{-/-}$ (J) showed a right-oriented aortic outflow with no apparent communication of the aorta with the LV. E11.5 control embryos (K), as well as $Fgf3^{-/-}$ (L), $Fgf10^{-/-}$ (N) and $Fgf3^{-/+}$;$Fgf10^{-/-}$ (O) mutant exhibited a patent OFT and normal myocardial wall thickness with robust trabeculation. (M) $Fgf3^{-/-}$;$Fgf10^{-/+}$ was the only genotype presenting at E11.5 with OFT occlusion (red arrow) and thin, poorly trabeculated ventricles. Scale bars in panels A, F and K apply to all panels in their respective columns. A = 400 μm; F, K = 200 μm.

(Figs. 3V and W) demonstrate the marked thin ventricular and atrial myocardium, and greatly reduced trabeculation in the double mutant (Fig. 3W). Such defects suggest cardiac insufficiency as a primary cause of double mutant lethality.

In addition to the defects found in the heart proper, the majority of the E10.5 3D-reconstructed double mutants appeared to lack a patent PAA4, suggesting a peripheral vascular defect. To evaluate the peripheral vasculature directly, we injected ink into the common ventricle at E10.5 and assessed its trajectory. Whereas PAA3, PAA4 and PAA6 were clearly patent in control embryos (Fig. 4A), PAA4 was not apparent in three of four double mutants (Fig. 4B). Analysis of histologic sections confirmed the absence, or lack of patency, of PAA4 in all three double mutants prepared at this stage, and this was associated with apparent failure of segmentation of the 4th pharyngeal arch (Figs. 4C and D). Thus, *Fgf3* and *Fgf10* are required redundantly for normal formation of the 4th pharyngeal arch and formation or stabilization of PAA4.

Taken together, the cardiovascular defects found in *Fgf3*/*Fgf10* double mutants are more severe than those found in *Fgfr2b* mutants (Marguerie et al., 2006), implicating additional FGF receptors in their pathogenesis. Furthermore, the abnormalities are indicative of perturbations in multiple cardiac progenitor cell populations.

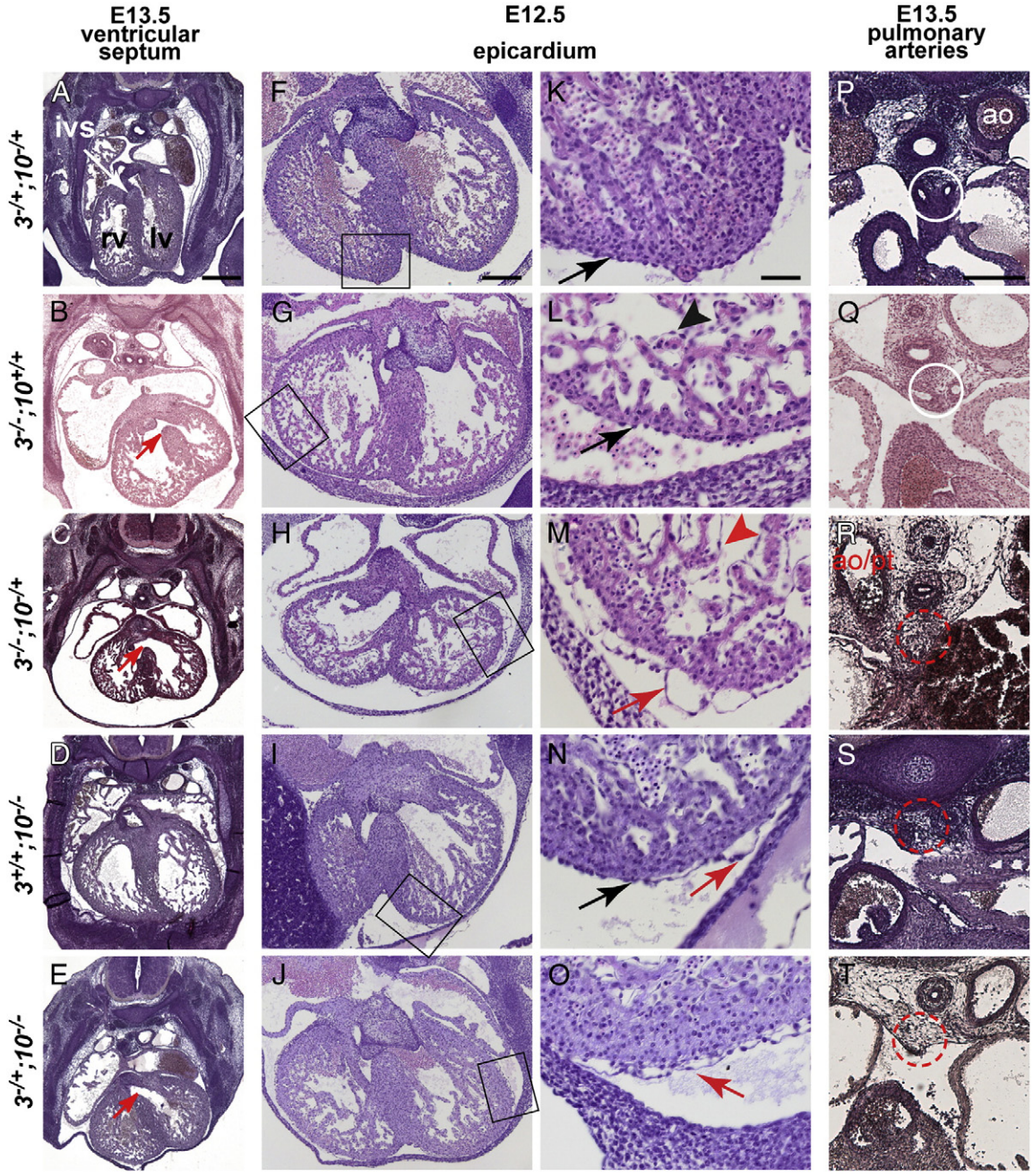

Fig. 2. Defects in ventricular septum formation, myocardial expansion, epicardial cell attachment and pulmonary artery formation are observed in embryos carrying combinations of three *Fgf3* and *Fgf10* null alleles. H&E-stained transverse sections of E12.5–E13.5 embryos. Genotypes are abbreviated to the left of each row as in Fig. 1. Embryonic age is indicated at the top of each column. (A–E) Sections taken through the middle of E13.5 hearts. (A) Control embryo demonstrating a normal interventricular septum (ivs) between the right (rv) and left (lv) ventricles. (B, C, E) Unfused ventricular septa (red arrows) were found in *Fgf3*$^{-/-}$, *Fgf3*$^{-/-}$;*Fgf10*$^{-/+}$ and *Fgf3*$^{-/+}$;*Fgf10*$^{-/-}$ embryos. The *Fgf3*$^{-/-}$;*Fgf10*$^{-/+}$ mutant (C) also shows thin atrial and ventricular myocardial walls and poor trabeculation. (F–O) Sections taken through the middle of E12.5 hearts and photographed at low magnification (F–J). Boxed region is enlarged in the adjacent panels (K–O). Control (F, K) and *Fgf3*$^{-/-}$ embryos (G, L) showed tight association of the epicardial layer with the underlying myocardium (K, L black arrows). One of three *Fgf10*$^{-/-}$ embryos (I, N) showed some epicardial detachment (red arrow; in contrast to tightly associated regions, black arrow). In contrast, in *Fgf3*$^{-/+}$;*Fgf10*$^{-/-}$ mutants (J, O) and even more strikingly in *Fgf3*$^{-/-}$;*Fgf10*$^{-/+}$ mutants (H, M) epicardial layers were very loosely attached to the myocardium (red arrows). Similarly, the endocardial layer in *Fgf3*$^{-/-}$;*Fgf10*$^{-/+}$ mutants (M, red caret) also showed poor association with the myocardium compared to the other genotypes (e.g., black caret in L). (P–T) Sections taken through the posterior pole of E13.5 hearts. Control (P) and *Fgf3*$^{-/-}$ (Q) embryos showed normal pulmonary artery development (two patent vessels inside white circle). *Fgf10*$^{-/-}$ (S), *Fgf3*$^{-/+}$;*Fgf10*$^{-/-}$ (T) and *Fgf3*$^{-/-}$;*Fgf10*$^{-/+}$ (R) mutants lacked pulmonary arteries (dotted red circle encloses expected location). Scale bars in panels A, F, K and P apply to all panels in their respective columns. A = 400 μm; F = 200 μm; K = 50 μm; P = 200 μm.

Fgf3 and Fgf10 are expressed in locations relevant to cardiovascular development

To correlate expression of *Fgf3* and *Fgf10* with the tissues relevant to normal cardiovascular development, we employed whole mount RNA in situ hybridization of E8.0–E10.5 embryos. At E8.0, *Fgf3* was detected in hindbrain neural ectoderm (ne), the preotic and pharyngeal ectoderm (poe, phe) and in pharyngeal pouch endoderm (ppe, Figs. 5A and A$_1$), each of which is adjacent to the origin and/or migration path of neural crest and second heart field mesoderm. At the same stage, *Fgf10* was expressed in the SHF (shf, Figs. 5E and E$_1$), which contributes primarily to the OFT, right ventricle and IFT (Dyer and Kirby, 2009; Rochais et al., 2009; Snarr et al., 2008). At E8.5, *Fgf3* persisted in neural ectoderm of rhombomeres 5 and 6, and in pharyngeal pouch endoderm (Figs. 5B and

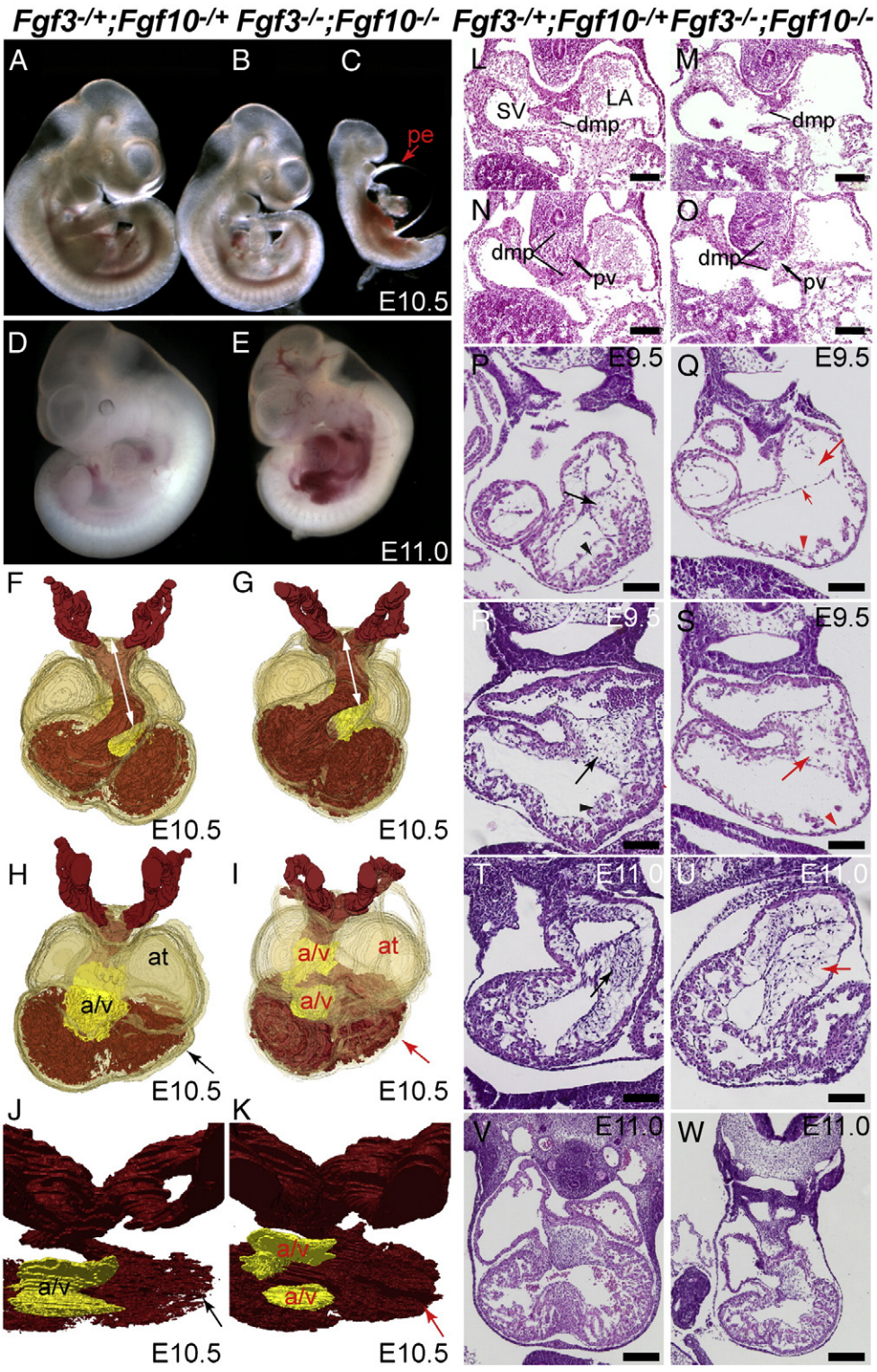

Fig. 3. *Fgf3*/*Fgf10* double null mutants have cardiovascular defects related to impaired development of the heart fields and neural crest. (A–C) Freshly dissected E10.5 $Fgf3^{-/+}$;$Fgf10^{-/+}$ (control) and $Fgf3^{-/-}$;$Fgf10^{-/-}$ (double mutant) embryos. Relative to controls (A), most double mutant littermates (B) were smaller, often with small pericardial effusions (pe) not obvious in this particular specimen. Other double mutant littermates showed striking cardiac malformations, such as a distended heart tube and large pe (C). (D–E) Freshly dissected E11.0–11.5 control and double mutant littermates. Relative to the control (D), there was significant blood pooling, a pericardial effusion, clearly thinned ventricles and poor to no heartbeat in the double mutant (E). (F–K) 3-D reconstructions of H&E-stained transverse sections of E10.5 control (F, H, J) and double mutant embryos (G, I, K) with blood-filled internal space pseudo-colored in red. Double mutant-specific defects included a shortened OFT (G, white arrow), dilated atria (at) and thin ventricles (red arrow) (I), and reduced trabeculation (K, red arrow) and unfused atrioventricular (a/v) cushions (I, K). (L–O) Transverse H&E-stained sections taken at two levels through E10.5 inflow tracts. Relative to controls (L, N), the anterior extent of the DMP was hypoplastic in double mutants (M). More posterior sections showed that double mutants had marked DMP hypoplasia (O; dmp cells lie between the lines) and that the DMP failed to fuse with the anterior IFT wall, leaving a persistent connection of the pulmonary vein (pv) to both the left atrium (LA) and sinus venosus (SV). (P–S) H&E-stained transverse sections of control and double mutant hearts at E9.5. Relative to anterior control sections (P, R), double mutants showed hypoplastic A/V cushions (Q, S red arrow) and thinned atrial and ventricular walls and poor trabeculation (Q, S red caret), and detached endocardium (Q short red arrow). Sections taken through E11.0 control (T, V) and double mutant (U, W) hearts showed hypocellular OFT cushions in double mutants (U, red arrow) and arrested, poorly developed myocardium with markedly reduced ventricular trabeculation (W). Panels L–U, scale bar = 100 μm; panels V–W, scale bar = 200 μm.

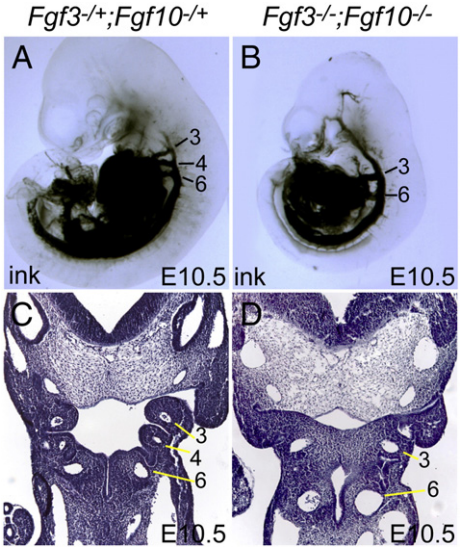

Fig. 4. *Fgf3/Fgf10* double null mutants fail to form a patent pharyngeal arch artery 4. (A, B) India ink injection into the common ventricle of E10.5 control (A) and double mutant (B) embryos showed that pharyngeal arch artery 4 was missing in double mutants. (C, D) H&E-stained coronal sections of E10.5 control (C) and double mutant (D) embryos revealed almost complete failure of 4th PA segmentation and severe 4th PAA hypoplasia in double mutants.

B_1), but was not expressed in more posterior neural ectoderm (Fig. 5B_2). At this stage, *Fgf10* expression initiated in the otic cup (adjacent to migrating neural crest) and in the first pharyngeal pouch endoderm, and persisted in pharyngeal mesoderm (pm, Figs. 5F_1 and F_2). At E9.5, *Fgf3* persisted in the neural ectoderm and pharyngeal pouch endoderm (Figs. 5C and C_1), whereas *Fgf10* persisted in the first pharyngeal pouch endoderm (1ppe) and pharyngeal mesoderm (Figs. 5G and G_1) and was initiated in the septum transversum and PEO (peo, Figs. 5G and G_2), which provides migratory progenitors for the epicardium and its derivatives (Lie-Venema et al., 2007; Ratajska et al., 2008; Reese et al., 2002). By E10.0, neurectodermal *Fgf3* expression ceased, but pharyngeal endodermal expression persisted (Figs. 5D and D_1) and *Fgf10* expression persisted in the anterior pharyngeal endodermal and mesodermal tissues (Figs. 5H and H_1) and in the PEO (Figs. 5H and H_2). Collectively, these data show that *Fgf3* and *Fgf10* are expressed dynamically in or immediately adjacent to tissues contributing to cardiovascular development, including the neural crest, pharyngeal ectoderm and endoderm, FHF and SHF and the PEO, with overlapping expression detected only in a small segment of the anterior pharyngeal endoderm.

Fgf3 and Fgf10 are required redundantly for deployment of postotic neural crest

Fgf3 is expressed in the hindbrain adjacent to the most anterior region from which the postotic neural crest emerges, and in both the pharyngeal endoderm and ectoderm adjacent to the migratory path of these cells as they contribute to cranial ganglia, pharyngeal arch arteries and the OFT septum. *Fgf10* is expressed in mesenchyme subjacent to the forming neural crest and in the pharyngeal endoderm. To determine whether *Fgf3* and *Fgf10* play roles in neural crest development, we stained E10.5 control and double null mutant embryos with Tuj1 antibody, which marks differentiated neurons, many of which are neural crest- or placode-derived at this stage (Figs. 6A and B). As expected, the double mutants lacked the otic placode-derived otic ganglion neurons (VIII; Figs. 6B and B_1) (Alvarez et al., 2003; Urness et al., 2010; Wright and Mansour, 2003). The double mutants also lacked the neural crest-derived glossopharyngeal ganglion neurons (proximal (p) IX^{th};), but retained the epibranchial placode-derived petrosal ganglion neurons (distal (d) IX^{th}; Figs. 6B and B_1). All of the other cranial ganglia (both neural crest- and epibranchial placode-derived) and trunk ganglia appeared normal in double mutants, and all cranial ganglia were normal in both $Fgf3^{-/-}$ and $Fgf10^{-/-}$ embryos (data not shown), suggesting a specific defect in postotic neural crest development in *Fgf3/Fgf10* double null mutants.

To determine whether the loss of glossopharyngeal ganglion neurons in double mutants resulted from failure of neural crest specification, migration or differentiation, we investigated a number of neural crest markers in control and double null mutant embryos between E8.5 and E10.5 (Figs. 6C–N). Expression of *Sox9* at E8.5 in newly specified neural crest cells located at the border of the neural and non-neural ectoderm, was not affected in double mutants (Figs. 6C and D). Similarly, expression of *Wnt1* at E9.0 in premigratory neural crest located along the entire dorsal aspect of the anteroposterior axis, was not affected in double mutants (Figs. 6E and F). The same was true at this stage for *Cadh6* and *Pax3* (data not shown). These results show that *Fgf3* and *Fgf10* are not required for neural crest specification.

Sox10 labels migratory neural crest and was expressed relatively normally at E9.0, when only preotic neural crest cells were migrating ventrally from r2 and r4 (white arrows; Figs. 6G and H). In contrast, relative to controls (Figs. 6I and K), E9.5–E10.5 *Fgf3/Fgf10* double mutants had much reduced *Sox10*-positive postotic neural crest (pnc) streams migrating away from r6 to form the IX–XI ganglia, or continuing to migrate through the pharyngeal arches and towards the heart (Figs. 6J and L). Similar results were obtained with a *Cadh6* probe (data not shown). In addition, the *Sox10*-expressing spur of neural crest that normally migrates into the fourth arch was absent (Figs. 6M and N), possibly reflecting the loss of the arch. Finally, since loss of *Fgf15* function leads to aberrant CNC behavior and consequent OFT and alignment defects (Vincentz et al., 2005), we examined its expression at E9.0 and E10.0, but observed no change in *Fgf3/Fgf10* double mutants (data not shown).

Taken together, these data show that *Fgf3* and *Fgf10* are required for normal migration and/or survival of a subset of neural crest, including that which contributes neurons and glia to the proximal ninth ganglia, participates in outflow tract septation and eventually contributes smooth muscle to PAA4. Furthermore, *Fgf3* and *Fgf10* function independently of effects on *Fgf15*.

Expression of Tbx1 and Fgf8 is unaffected in Fgf3/Fgf10 double null mutants

Anomalies of PAA4 and outflow tract development similar to those seen in the *Fgf3/Fgf10* double mutants occur commonly in humans with DiGeorge and other 22q11 deletion syndromes and are phenocopied in mice bearing mutations in *Tbx1* or *Fgf8* (Abu-Issa et al., 2002; Frank et al., 2002; Lindsay et al., 2001). Indeed, *Tbx1* and *Fgf8* genetically interact in the development of PAA4 (Aggarwal et al., 2006; Vitelli et al., 2002). Therefore, to determine whether cardiovascular phenotypes of *Fgf3/Fgf10* double mutants were related to misregulation of *Tbx1* and/or *Fgf8*, we examined their expression in the pharyngeal region of control and double mutant embryos. Neither gene was affected in double mutants from E8.5–10.5 (Figs. 7A–F and data not shown), even when 4th pharyngeal arch hypoplasia was obvious (Fig. 7F_1).

Wnt11 is a target of *Fgf8* (Park et al., 2006; Park et al., 2008) and a marker of the OFT (Cai et al., 2003) that is required for OFT alignment and septation (Zhou et al., 2007), however, neither *Wnt11* nor *Tdgf1* (*Cripto*), another OFT-expressed gene (Xu et al., 1999), was misregulated in *Fgf3/Fgf10* double mutants (Suppl. Fig. 2). These data suggest that the requirement for *Fgf3* and *Fgf10* in cardiovascular development is independent or downstream of *Tbx1* and *Fgf8*.

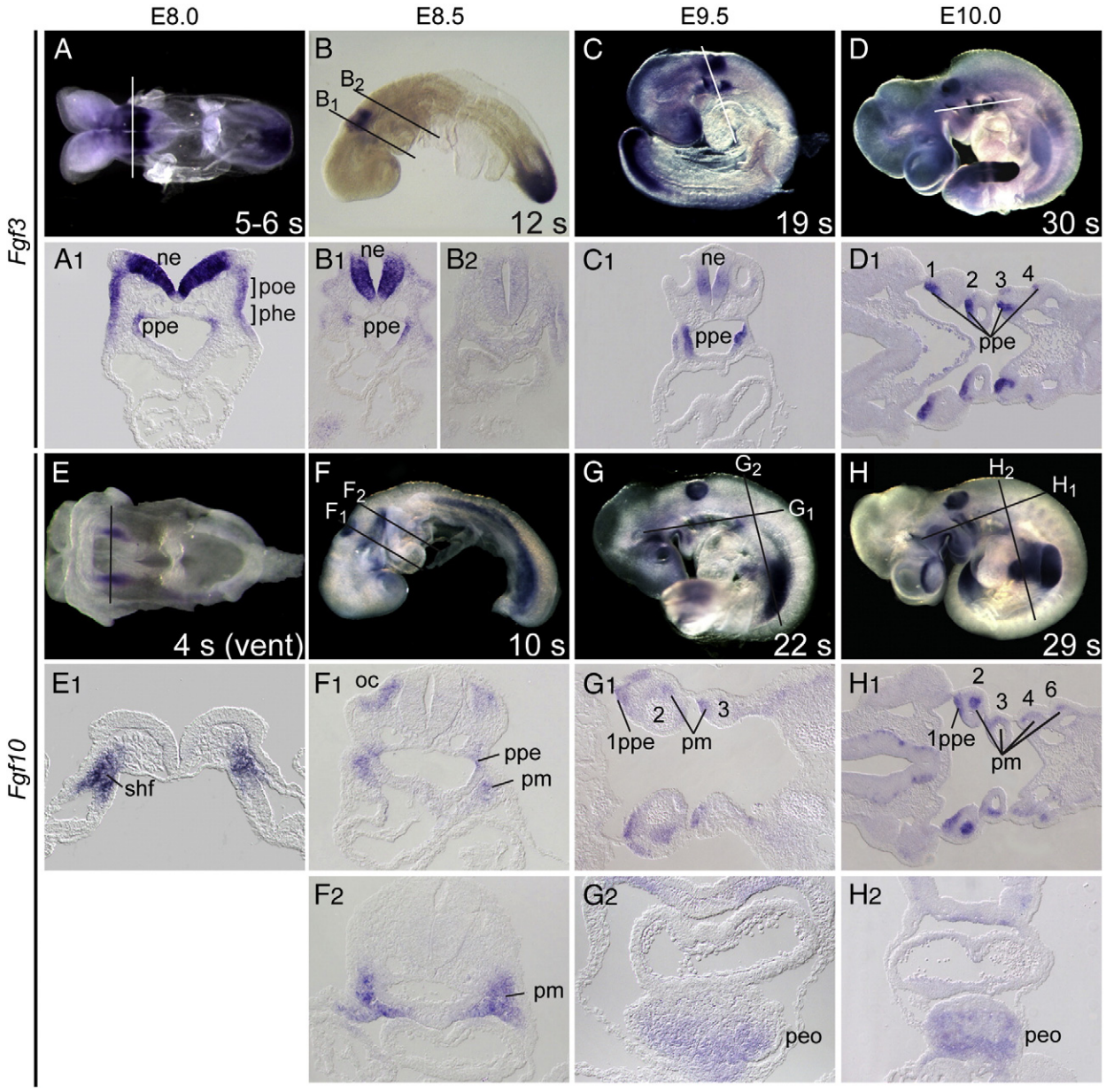

Fig. 5. *Fgf3* and *Fgf10* are expressed in locations relevant to cardiovascular development. Whole-mount in situ hybridization of wild type embryos using *Fgf3* (A–D) or *Fgf10* (E–H) probes at E8.0–E10.0. A line indicates the plane of cryosections shown below each whole mount. *Fgf3* transcripts were found in pharyngeal pouch endoderm (ppe) from E8.0–E10.0 (A_1, B_1, C_1, D_1), in preotic ectoderm (poe) at E8.0 (A_1), and hindbrain rhombomeres 5 and 6 neural ectoderm (ne) from E8.0–E9.5 (A_1, B_1, C_1), but not in more posterior ne (B_2). *Fgf10* was found in the second heart field (shf) at E8.0 (E_1), initiated in the ppe at E8.5 (F_1), and persisted in the pharyngeal mesoderm (pm) and endoderm at E8.5–E10.0 (F_1, F_2, G_1, H_1). Otic cup (oc) expression of *Fgf10* was apparent at E8.5 (F_1) and ppe expression was weak at E9.5–E10.0 (G_1, H_1). *Fgf10* expression in the proepicardial organ (peo) was observed at E9.5–E10.0 (G_2, H_2).

Critical transcriptional regulators of cardiac mesoderm development are perturbed in Fgf3/Fgf10 double mutants

Fgf3 and *Fgf10* are required for and are expressed in or near the developing FHF and SHF, so we examined molecular markers of these progenitor populations and their descendants in control and double mutant embryos (Fig. 8). *Nkx2-5* encodes a critical transcriptional regulator of the cardiac myogenic program (Ponticos, 2010). Its expression was dramatically reduced in both atrial and ventricular cardiomyocytes in two of three E10.5 double mutants (Figs. 8A, A_1, B, B_1). Surprisingly, *Nkx2-5* expression appeared normal at E9.5 (Figs. 8C and D) and at E8.5 (data not shown). Expression of other cardiomyocyte developmental markers, including *Myl7* (*Mlc2a*), *Mef2c*, *Hand2* (*dHand*) and *Nappa (Anf)*, was not altered in double mutants (Suppl. Fig. 3), suggesting that the effect on *Nkx2-5* may be on the number of transcripts per cell, rather than a consequence of reduced numbers of cardiomyocytes or global decline in transcription.

Isl1 is expressed in and required for development of the SHF (Cai et al., 2003). *Isl1* SHF expression in double mutants was normal at E10.5 (data not shown) and at 19–20 somites (Figs. 8E and F), a half-day prior to the first morphologic manifestations of *Fgf3/Fgf10* deficiency. In contrast, *Isl1* expression was absent from the second heart field in three of three E8.0 double mutant embryos (7–8 somites, Figs. 8G and H and 4 somites Figs. 8I and J). However, *Isl1* expression was robust in the double mutant cardiac crescent at the 2–3-somite stage (Figs. 8K and L). Thus, *Isl1* expression appears to be transiently dependent upon *Fgf3* and *Fgf10* between the 4- and 20-somite stages, but may be regulated by other factors prior and subsequent to this developmental window.

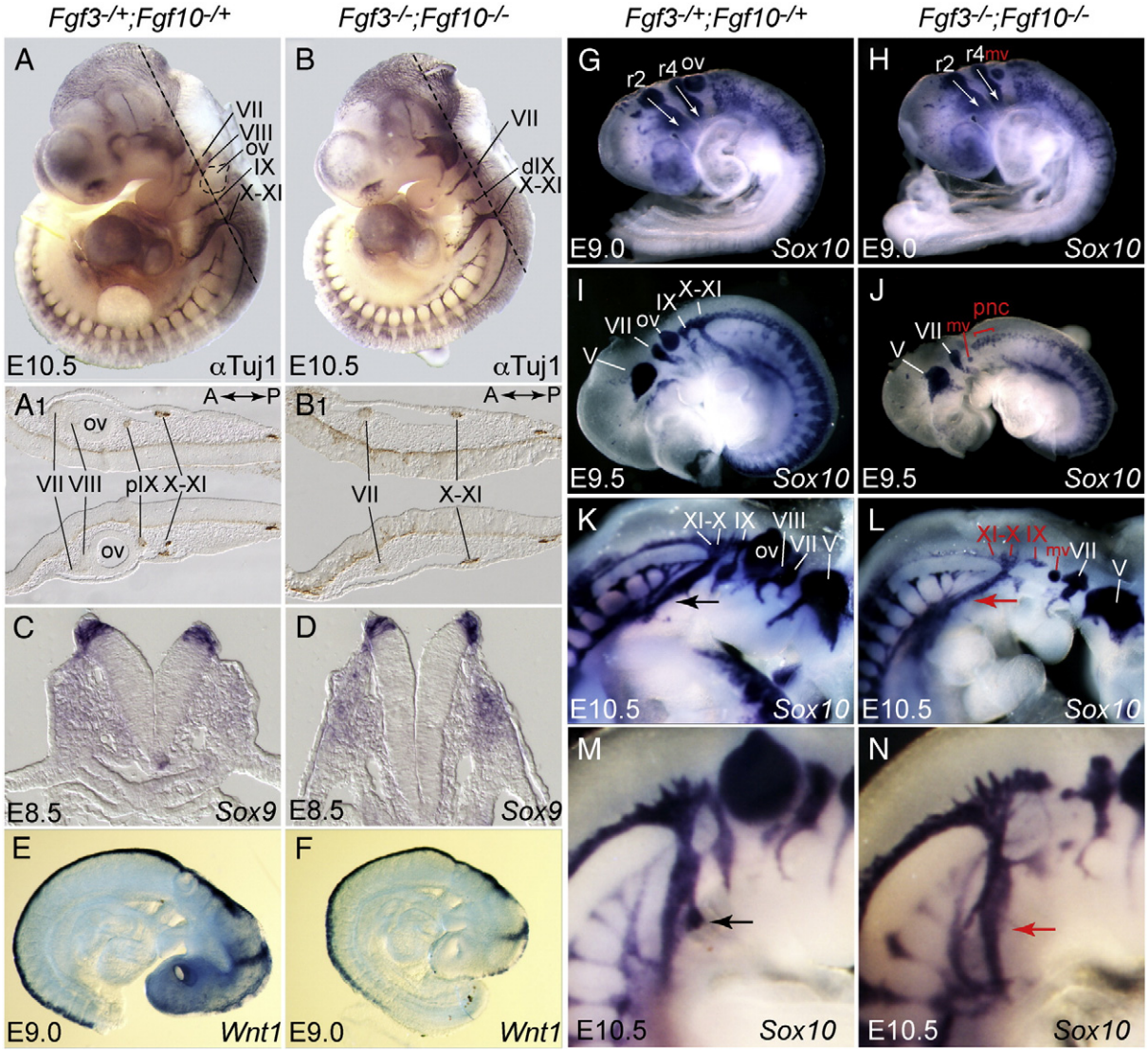

Fig. 6. *Fgf3* and *Fgf10* are required redundantly for deployment of post-otic neural crest. Whole mount immunohistochemistry with Tuj1 antibody labeled differentiated neurons in E10.5 control (A) and double mutant (B) embryos. Dotted lines indicate the plane of cryosections shown below each embryo (A_1, B_1). Relative to controls (A, A_1), double mutants lacked the otic ganglion (VIII) and the neural crest-derived proximal glossopharyngeal ganglion (pIX), but retained the epibranchial placode-derived petrosal ganglion (dIX) (B, B_1). Whole mount in situ hybridization of control and double mutant embryos with *Sox9* at E8.5 (C, D), *Wnt1* at E9.0 (E, F) and *Sox10* at E9.0 (G, H) showed that neural crest specification and early migration occurred normally in double mutants. In contrast, expression of *Sox10* at E9.5–E10.5 (I–N) revealed that postotic neural crest migrating distally from the neural tube and through the pharyngeal arches towards the heart was reduced in double mutants (J, L, red arrow). *Sox10*-positive cells were markedly reduced in the IX^{th} ganglion as well as in the X^{th} and XI^{th} ganglia (red labels in L). A higher magnification view of the E10.5 pharyngeal region showed that *Sox10* marks a spur of neural crest transiting the 4th arch in the control embryo (M, black arrow) that was absent from the double mutant (N, red arrow). Abbreviations: mv, micro-otic vesicle; ov, otic vesicle; pnc, post-otic neural crest; r2, r4, rhombomeres 2, 4; V–XI refer to forming ganglia.

Since *Fgf10* is itself a marker of the SHF that depends on *Isl1* expression (Cai et al., 2003), and transcripts from the $Fgf10^{\Delta 2}$ (exon 2 deletion) allele we used are stable (RT-PCR data not shown), we were able to test their expression as well. Like *Isl1*, $Fgf10^{\Delta 2}$ transcripts were unaffected in E9.5 double mutants (Figs. 8M and N), but were absent or somewhat reduced in two of three 5–7-somite (E8.0) double mutants (Figs. 8O and P). Similar to *Isl1*, $Fgf10^{\Delta 2}$ transcripts were strongly expressed in the cardiac crescent in 2–3-somite double mutant embryos (Figs. 8Q and R).

Fgf8 is also required for SHF development and is needed prior to E8.5 for normal levels of *Isl1* expression (Park et al., 2006). Therefore, we examined *Fgf8* expression at several additional stages, prior to the decrease in *Isl1* expression, but no differences between control and double mutant embryos were apparent, even in 1-somite embryos (Figs. 8S and T), when the SHF is forming. Expression of *Bmp4*, a prominent mediator of *Fgf8* signaling in the OFT myocardium, was also unaffected in the OFT or chamber myocardium of *Fgf3*/*Fgf10* double mutants in E9.5–10.5 embryos (data not shown).

Taken together, morphologic and marker analyses suggest that *Fgf3* and *Fgf10* are not required to specify cardiac progenitors, but are coordinately required to effect normal cellular contributions to the developing heart from both the SHF and postotic neural crest and that this requirement is independent of *Fgf8*.

Proepicardial cell deployment is reduced or delayed in Fgf3/Fgf10 double mutants

The epicardium surrounding the heart is comprised of a thin layer of cells mainly derived from the PEO, which develops at the base of the heart on the anterior surface of the septum transversum. These cells migrate anteriorly to ensheathe most of the developing myocardium by E11.0. There is also a small population of epithelial cells in the

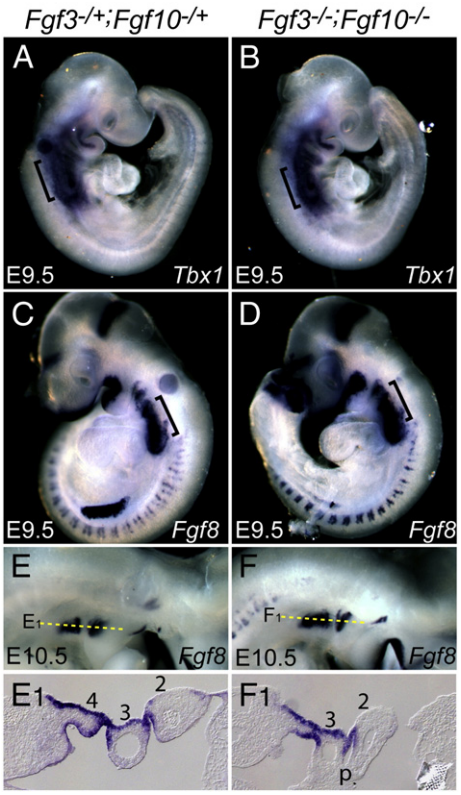

Fig. 7. Expression of *Tbx1* and *Fgf8* is unaffected in *Fgf3/Fgf10* double null mutants. In situ hybridization of control and double mutant embryos with *Tbx1* and *Fgf8*. Relative to controls (A, C, E, E_1), there was no difference in double mutant embryos with respect to expression of *Tbx1* at E9.5 (B) or *Fgf8* at E9.5 (D) and E10.5 (F, F_1), even when the double mutant 4th PA was clearly hypoplastic (F_1). In E, F dorsal is up, anterior to the right, and dotted lines indicate the plane of coronal sections shown in E_1, F_1.

vicinity of the SHF that gives rise to epicardial cells that ensheathe the distal OFT (Pérez-Pomares et al., 2003). The epicardium plays a vital role in stimulating the proliferation of cardiomyocytes, and contributing to the coronary vessels and fibrous interstitium of the maturing heart (Männer et al., 2001; Ratajska et al., 2008; Virágh and Challice, 1981). Since triple-allelic mutants showed epicardial detachment, and *Fgf10* is expressed in the PEO at E9.5 (Figs. 5G–H_2), we assessed the development of this unique cell population in double mutants. Examination of epicardial cell markers, *Tcf21* (Figs. 9A–B_2) and *Tbx18* (data not shown) in E10.5 embryos, showed that, relative to control embryos (Figs. 9A_1 and A_2), double mutants had fewer epicardial cells encasing the developing OFT (Fig. 9B_1) and ventricles (Fig. 9B_2). However, at E9.5, expression of PEO markers *Gata4* (Figs. 9C–D_1) and *Wnt2a* (data not shown) was normal in double mutants, as was PEO gross morphology (data not shown). Thus, *Fgf3* and *Fgf10* are necessary for epicardial cell development after the PEO is specified.

Discussion

Previous morphologic and molecular marker analyses of mouse embryos lacking expression of three or all four alleles of *Fgf3* and *Fgf10* revealed critical redundant and dosage sensitive roles for these genes in initiating inner ear development (Alvarez et al., 2003; Ladher et al., 2005; Wright and Mansour, 2003). The present analyses of such embryos show that *Fgf3* and *Fgf10* also play redundant and dosage sensitive roles in cardiovascular development. We found that removing one copy of *Fgf3* from the *Fgf10* null background causes OFT alignment and rotation defects, VSD and moderate epicardial detachment. Removing one copy of *Fgf10* from the *Fgf3* null background causes OFT and rotation defects and, in one case, PTA. These embryos also displayed VSD, thin and poorly trabeculated ventricular myocardium, severe epicardial detachment, pulmonary artery aplasia and lung hypoplasia. These phenotypes have variable penetrance and expressivity, with the $Fgf3^{-/-};Fgf10^{-/+}$ genotype causing earlier lethality and more severe and penetrant cardiovascular phenotypes than does the $Fgf3^{-/+};Fgf10^{-/-}$ genotype. Indeed, the $Fgf3^{-/-};Fgf10^{-/+}$ phenotypes are almost as severe as those of the double mutants, which strikingly, all die at E11.5, exhibiting thin and poorly trabeculated ventricular and atrial myocardium. This presumably renders the heart unable to pump adequately and is the most likely cause of embryonic demise. Other variably penetrant defects in double mutants include absence of PAA4 and sometimes the entire fourth pharyngeal arch, slightly shortened OFT, and a hypoplastic DMP and OFT cushions. While serious, these defects are generally compatible with survival to birth.

How do the *Fgf3/Fgf10* double mutant cardiovascular phenotypes arise? A model summarizing the expression patterns of *Fgf3* and *Fgf10* at two stages, and how they might signal to cardiovascular progenitors is shown in Fig. 10. We propose that redundancy between *Fgf3* expressed from the hindbrain and *Fgf10* expressed from the SHF is required for normal deployment of postotic neural crest, leading to loss of the proximal, neural crest-derived component of the glossopharyngeal ganglion and failure of PAA4 to persist in double null mutants, but not in *Fgf3* or *Fgf10* single null mutants. The PAA4 phenotype is similar to that observed following cardiac neural crest ablation in chick embryos (Waldo et al., 1996) or loss of *Fgf8* from mouse embryos (Abu-Issa et al., 2002; Frank et al., 2002; Macatee et al., 2003). When either an *Fgf3* or *Fgf10* wild type allele remains (i.e. in $Fgf3^{-/+};Fgf10^{-/-}$ or $Fgf3^{-/-};Fgf10^{-/+}$ embryos), there is sufficient signal for proximal glossopharyngeal ganglion and PAA4 development, but the CNC must still be somewhat impaired, leading to PTA and/or VSD, evident at stages after double mutants die. Since neural crest-restricted ablation of *Fgfr1* and *Fgfr2* (Park et al., 2008), encoding the major receptors for FGF3 and FGF10, or of *Frs2α* (Zhang et al., 2008), encoding an adaptor protein linking FGF receptors to the MAPK and PI3 kinase pathways, does not disrupt CNC contribution to the growing OFT, it is likely that FGF3 and FGF10 act indirectly on neural crest. They could, for example, regulate SHF-expressed *Bmp* genes, which are required to activate signaling through BMP receptors and SMAD4 for normal development of neural crest as well as the SHF (Azhar et al., 2010; McCulley et al., 2008; Qi et al., 2007; Song et al., 2007; Yang et al., 2006). Indeed, some of the gross phenotypes seen in *Fgf3/Fgf10* double mutants are similar to those of neural crest-specific ablation of *Bmpr1a* (Nomura-Kitabayashi et al., 2009; Stottmann et al., 2004) or *Smad4* (Jia et al., 2007; Ko et al., 2007; Nie et al., 2008). Although we did not find any change in myocardial *Bmp4* expression in the double mutants, there are several other candidates, including *Bmps 2*, *6*, *7* and *10* that could be affected. However, if FGF signaling affects expression of multiple *Bmps*, each to only a small extent, such differences would be difficult to detect.

Although the effects of *Fgf3/Fgf10* abrogation on postotic neural crest are likely to be indirect, we have evidence for direct effects of these signals on the SHF. *Isl1*, a key regulator of SHF development, was transiently down-regulated at E8.5, and *Nkx2-5* expression was reduced only at E10.5, when other cardiomyocyte markers were normally expressed. These results suggest that FGF3/FGF10 signals are probably not required to initiate expression of these genes, but may play important stage-specific roles in their subsequent regulation. The consequences of a transient disruption of *Isl1* expression have not been reported previously, but this gene regulates many SHF genes, including *Fgf10* (Cai et al., 2003). Indeed, we found that the $Fgf10^{\Delta 2}$ mutant transcript was absent or reduced in double mutants at E8.5, but not at later stages. The interruption of *Isl1* expression could lead to transient alterations in additional target genes sufficient to delay or discoordinate second heart field development relative to the neural crest. The shortened OFT and hypoplastic DMP in *Fgf3/Fgf10* double

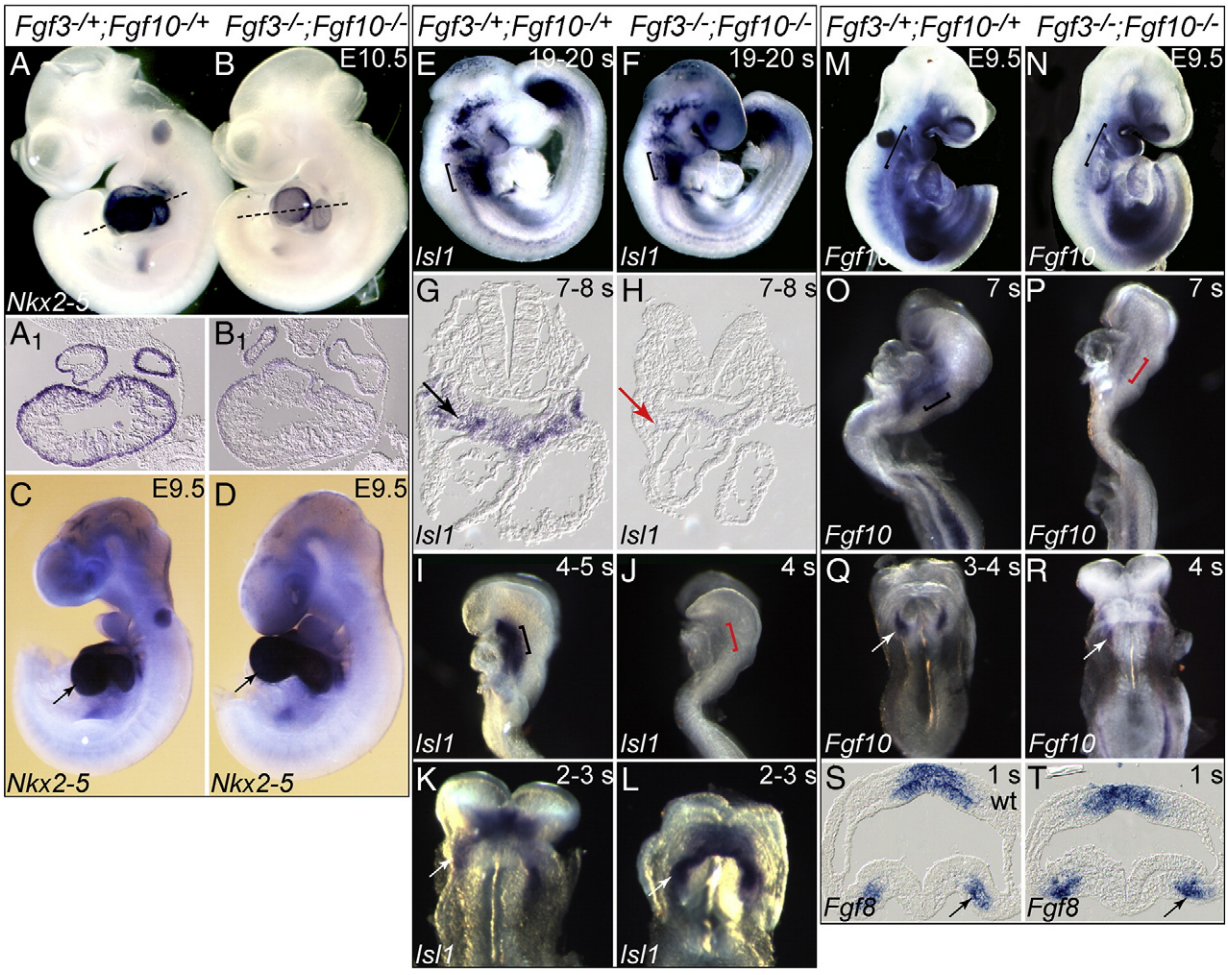

Fig. 8. Markers of cardiac mesoderm development are transiently perturbed in *Fgf3*/*Fgf10* double null mutants. In situ hybridization of control and double mutant embryos with *Nkx2-5*, *Isl1*, *Fgf10* and *Fgf8*. Relative to control embryos (A) *Nkx2-5* expression was strongly reduced in double mutant hearts (B). Black lines indicate the plane of sections shown in A_1, B_1. Expression of *Nkx2*-5 was comparable in E9.5 control and double mutant hearts (C, D; black arrows). Pharyngeal region *Isl1* expression (bracketed) was similar in 19–20-somite control (E) and double mutant embryos (F). In contrast, although *Isl1* expression in the SHF of 7–8-somite controls was robust (G; black arrow), it was absent from the double mutant SHF (H; red arrow). Similarly, SHF *Isl1* expression was robust in 4–5-somite controls (I; black bracket), but absent from double mutants (J; red bracket). *Isl1* was expressed normally in the cardiac crescent of both 2–3-somite controls (K) and double mutants (L). Expression of the $Fgf10^{\Delta 2}$ transcript in the pharyngeal region and right ventricle of E9.5 control and double mutants was similar (M, N; brackets). In contrast, while control 7-somite embryos showed stable $Fgf10^{\Delta 2}$ transcripts in pharyngeal mesoderm (O; black bracket,), they were less abundant in double mutant embryos (P; red bracket). $Fgf10^{\Delta 2}$ transcripts were expressed similarly in the cardiac crescent of both 3–4-somite control and double mutant embryos (Q, R). *Fgf8* expression in the cardiac crescent was comparable in 1-somite control (wild type) (S) and double mutant embryos (T).

mutants are consistent with this idea. Similarly, the reduced expression at E10.5 of *Nkx2-5*, a key regulator of the cardiomyogenic program in both FHF and SHF derivatives, could contribute to the thin and poorly trabeculated walls of the *Fgf3*/*Fgf10* double mutant ventricular myocardium. However, the late timing of the *Nkx2-5* loss suggests that it is not likely to be the primary cause of the myocardial phenotype.

The morphologic and molecular defects found in *Fgf3*/*Fgf10* double mutant cardiac development do not occur in *Fgf10* null mutants (Marguerie et al., 2006), pointing to a key role for *Fgf3* in their pathogenesis. Since *Fgf3* is expressed at early stages in the hindbrain and endoderm located in close proximity to the SHF, the FGF3 signal functioning redundantly with FGF10 to control SHF development could arise from either or both locations. It is tempting to ascribe all of the double mutant phenotypes to loss of *Fgf3* from the hindbrain and *Fgf10* from the SHF, leading to postotic neural crest deficits and consequent discoordination of CNC and SHF development. However, given the important roles already described for FGF signaling from the endoderm to the SHF (Park et al., 2008; Zhang et al., 2008), potential roles for endodermal *Fgf3* should not be discounted, and can be tested using conditional gene ablation approaches.

SHF-expressed FGF8 is a key autocrine regulator of OFT development (Ilagan et al., 2006; Park et al., 2006) and *Fgf10* transcripts are reduced in the SHF of *Fgf8* hypomorphic embryos (Abu-Issa et al., 2002; Frank et al., 2002). Recent data show that the penetrance of PAA4 as well as OFT defects in SHF conditional *Fgf8* mutants is increased by removal of *Fgf10* alleles (Watanabe et al., 2010). Combined with our previously published data showing that splanchnic mesodermal expression of *Fgf10* is reduced or absent in E8.0 *Fgf3* null/*Fgf8* hypomorphic embryos (Ladher et al., 2005) and that *Fgf8* expression is unaffected in similarly staged *Fgf3*/*Fgf10* double null mutants (this paper), we suggest that, as in otic placode induction, *Fgf8* functions upstream of *Fgf10* during sequential phases of FGF signaling in cardiovascular development, and that *Fgf3* functions redundantly with each of these *Fgfs*.

In addition to effects on the neural crest and myocardium, we found that *Fgf3*/*Fgf10* double mutant hearts have reduced epicardial cell ensheathment and the triple-allelic mutants, particularly $Fgf3^{-/-}$; $Fgf10^{-/+}$, showed detachment of epicardial cells from the myocardium. Epicardial cells are proposed to play important roles in at least stimulating myocardial growth and possibly in providing additional cells to the myocardium, in addition to their ultimate fate as progenitors of coronary vessels and interstitium (Carmona et al.,

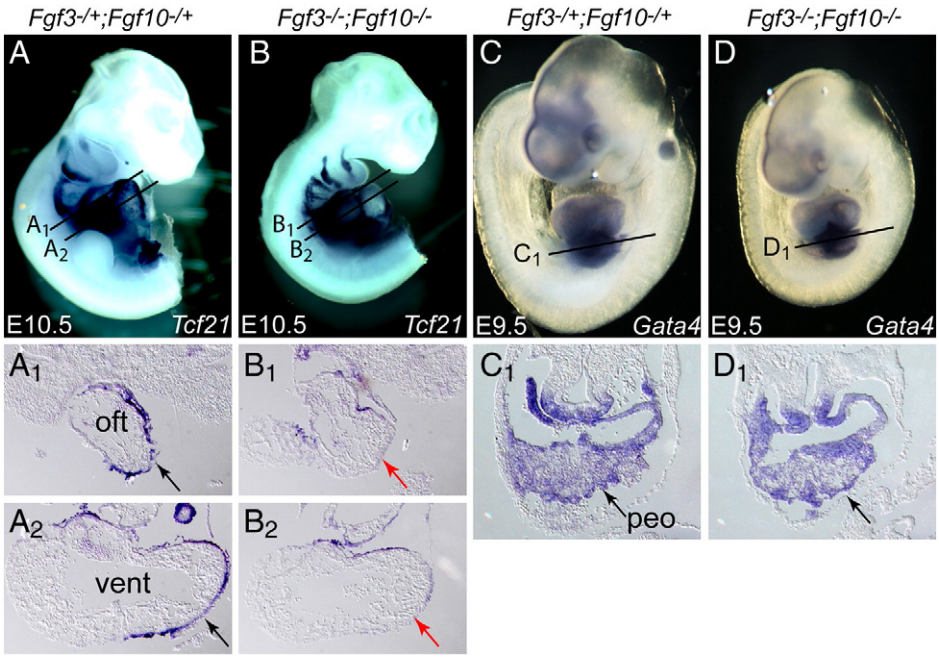

Fig. 9. *Fgf3* and *Fgf10* are required redundantly for normal epicardial cell deployment over the heart, but not for initial specification of the proepicardial organ. (A–D) Whole mount in situ hybridization of control and double mutant embryos with epicardial markers *Tcf21* (*Epicardin*) and *Gata4*. Lines through each embryo indicate the planes of sections shown below each embryo. Relative to control embryos, which showed robust ensheathment of the OFT and ventricles with *Tcf21*-positive epicardial cells (A_1, A_2 black arrows), the double mutant OFT (B_1, red arrow) and ventricle (B_2, red arrow) were deficient in such cells. No differences with respect to *Gata4* expression (black arrows) were apparent between control (C, C_1) and double mutant (D, D_1) embryos.

2010; Gittenberger-de Groot et al., 2010; Ratajska et al., 2008). Indeed, ablation of the chick PEO, the major source of epicardial cells, leads to thin myocardium in addition to loss of the coronary vasculature (Männer et al., 2005; Pérez-Pomares et al., 2002). However, impairment of epicardial cell function seems unlikely to be the sole cause of the myocardial phenotype and early demise of *Fgf3*/*Fgf10* double mutant embryos, which occurs prior to established critical roles for the epicardium. However, such an early functional role for the mouse epicardium cannot be discounted and could be addressed directly by genetic ablation of the PEO lineage.

Another question concerning the epicardial phenotype described here is whether it is a direct or indirect consequence of loss of *Fgf3* and *Fgf10*. *Fgf10* is certainly expressed in the PEO and could stimulate its proliferation, as proposed in chick (Torlopp et al., 2010), or its

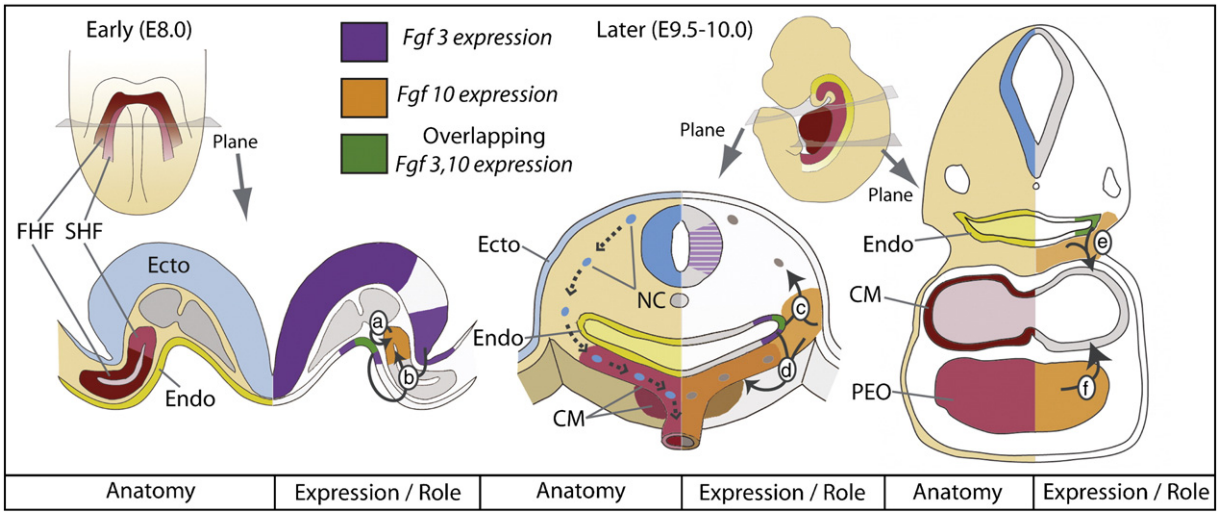

Fig. 10. Model for *Fgf3* and *Fgf10* expression and function during cardiovascular development. Embryonic structures and expression of *Fgf3* and *Fgf10* (left and right of sectional views, respectively) are shown at E8.0 and E9.5–10.0. At early stages, *Fgf10* expression in the SHF (red) could be directly required for SHF development (arrow a) in conjunction with *Fgf3* expressed from the hindbrain (purple) and/or endoderm, which also expresses *Fgf10* (green) (arrow b). An indirect effect of FGF3/FGF10 signaling to SHF could be perturbation of signals required for subsequent neural crest (NC) development. Both *Fgf3* and *Fgf10* are also expressed at later stages, and could continue to influence cardiovascular development. *Fgf3* and *Fgf10* expressed in the pharyngeal endoderm (green), and with or without *Fgf10* expression from the pharyngeal mesoderm (orange), could indirectly affect the migratory NC (arrow c) and/or the cardiogenic mesoderm (CM, arrows d, e). Although there is no source of *Fgf3* in the vicinity of the proepicardial organ (PEO), earlier redundant FGF3/FGF10 signals to the SHF could be required with PEO-expressed *Fgf10* (arrow f) to regulate ensheathment of the heart by migrating proepicardial cells. Alternatively, contributions of FGF10 signals from the PEO could influence the CM. Abbreviations: Ecto, ectoderm (blue); Endo, endoderm (yellow); CM, cardiogenic mesoderm; FHF, first heart field; NC, neural crest; PEO, proepicardial organ; SHF, second heart field.

migratory behavior, or even its ability to adhere to the myocardium, but it must do so in conjunction with *Fgf3*, which is not expressed near the PEO at times when the phenotype is observed. Another possibility is that the failure of myocardial ensheathment by proepicardial cells is an indirect consequence of a "sick" myocardium caused more directly by loss of FGF3/FGF10 signaling to the early progenitors of the myocardium (i.e. in the FHF and SHF). Resolving this issue will require conditional analyses.

What is the relevance of our findings to the etiology of congenital heart defects in humans? Mutations in *FGF3* and *FGF10* are each associated with multiple malformation syndromes. Homozygosity for recessive loss-of-function mutations in *FGF3* causes LAMM (labyrinthine aplasia–microdontia–microtia) syndrome (Tekin et al., 2008) and those in *FGF10* cause LADD (lacrimo-auriculo-dento-digital) syndrome (Rohmann et al., 2006). Neither of these very rare syndromes has been associated with heart defects; however, neither gene has been examined in large groups of patients with isolated heart defects. Furthermore, the convergence of inner ear and cardiovascular developmental defects in double mutant mouse embryos has parallels with human syndromes such as DiGeorge and CHARGE, which are caused, in part, by mutations in *TBX1* and *CHD7*, respectively, and are modeled in *Tbx1*, *Fgf8* and *Chd7* mutant mice. We suggest that *FGF3* and *FGF10* should now be considered candidates for genes that when mutated or misregulated contribute to isolated heart defects, and particularly to congenital syndromes presenting with cardiovascular defects and hearing loss.

Supplementary materials related to this article can be found online at doi:10.1016/j.ydbio.2011.05.671.

Acknowledgments

We thank Albert Noyes for superb technical support, and particularly for the *Fgf8* ISH on 1-somite embryos, and Katie Barrows, Sam Gliford and Jennifer Hunter for help with histology and heart reconstructions. We thank Yukio Saijoh for helpful comments on the manuscript. In addition, we are grateful to the numerous colleagues who supplied probes for ISH. This work was supported by grants from the American Heart Association (0755150Y, S.L.M.) and the NIH (DC004185, S.L.M.; HL084559, S.B.B; HD044157, A.M.M).

References

Abu-Issa, R., Kirby, M.L., 2007. Heart field: from mesoderm to heart tube. Annu. Rev. Cell Dev. Biol. 23, 45–68.
Abu-Issa, R., Smyth, G., Smoak, I., Yamamura, K., Meyers, E.N., 2002. *Fgf8* is required for pharyngeal arch and cardiovascular development in the mouse. Development 129, 4613–4625.
Aggarwal, V.S., Liao, J., Bondarev, A., Schimmang, T., Lewandoski, M., Locker, J., Shanske, A., Campione, M., Morrow, B.E., 2006. Dissection of Tbx1 and Fgf interactions in mouse models of 22q11DS suggests functional redundancy. Hum. Mol. Genet. 15, 3219–3228.
Alvarez, Y., Alonso, M.T., Vendrell, V., Zelarayan, L.C., Chamero, P., Theil, T., Bösl, M.R., Kato, S., Maconochie, M., Riethmacher, D., Schimmang, T., 2003. Requirements for FGF3 and FGF10 during inner ear formation. Development 130, 6329–6338.
Azhar, M., Wang, P.Y., Frugier, T., Koishi, K., Deng, C., Noakes, P.G., McLennan, I.S., 2010. Myocardial deletion of *Smad4* using a novel alpha skeletal muscle actin Cre recombinase transgenic mouse causes misalignment of the cardiac outflow tract. Int. J. Biol. Sci. 6, 546–555.
Bleyl, S.B., Saijoh, Y., Bax, N.A., Gittenberger-de Groot, A.C., Wisse, L.J., Chapman, S.C., Hunter, J., Shiratori, H., Hamada, H., Yamada, S., Shiota, K., Klewer, S.E., Leppert, M.F., Schoenwolf, G.C., 2010. Dysregulation of the *PDGFRA* gene causes inflow tract anomalies including TAPVR: integrating evidence from human genetics and model organisms. Hum. Mol. Genet. 19, 1286–1301.
Brown, C.B., Wenning, J.M., Lu, M.M., Epstein, D.J., Meyers, E.N., Epstein, J.A., 2004. Cre-mediated excision of *Fgf8* in the *Tbx1* expression domain reveals a critical role for *Fgf8* in cardiovascular development in the mouse. Dev. Biol. 267, 190–202.
Bruneau, B.G., 2008. The developmental genetics of congenital heart disease. Nature 451, 943–948.
Cai, C.L., Liang, X., Shi, Y., Chu, P.H., Pfaff, S.L., Chen, J., Evans, S., 2003. Isl1 identifies a cardiac progenitor population that proliferates prior to differentiation and contributes a majority of cells to the heart. Dev. Cell 5, 877–889.
Carmona, R., Guadix, J.A., Cano, E., Ruiz-Villalba, A., Portillo-Sánchez, V., Pérez-Pomares, J.M., Munoz-Chápuli, R., 2010. The embryonic epicardium: an essential element of cardiac development. J. Cell. Mol. Med. 14, 2066–2072.
Chien, K.R., Domian, I.J., Parker, K.K., 2008. Cardiogenesis and the complex biology of regenerative cardiovascular medicine. Science 322, 1494–1497.
Chisaka, O., Musci, T.S., Capecchi, M.R., 1992. Developmental defects of the ear, cranial nerves and hindbrain resulting from targeted disruption of the mouse homeobox gene *Hox-1.6*. Nature 355, 516–520.
Conway, S.J., Kruzynska-Frejtag, A., Kneer, P.L., Machnicki, M., Koushik, S.V., 2003. What cardiovascular defect does my prenatal mouse mutant have, and why? Genesis 35, 1–21.
Dyer, L.A., Kirby, M.L., 2009. The role of secondary heart field in cardiac development. Dev. Biol. 336, 137–144.
Frank, D.U., Fotheringham, L.K., Brewer, J.A., Muglia, L.J., Tristani-Firouzi, M., Capecchi, M.R., Moon, A.M., 2002. An *Fgf8* mouse mutant phenocopies human 22q11 deletion syndrome. Development 129, 4591–4603.
Gittenberger-de Groot, A.C., Winter, E.M., Poelmann, R.E., 2010. Epicardium-derived cells (EPDCs) in development, cardiac disease and repair of ischemia. J. Cell. Mol. Med. 14, 1056–1060.
Goddeeris, M.M., Rho, S., Petiet, A., Davenport, C.L., Johnson, G.A., Meyers, E.N., Klingensmith, J., 2008. Intracardiac septation requires hedgehog-dependent cellular contributions from outside the heart. Development 135, 1887–1895.
Hatch, E.P., Noyes, C.A., Wang, X., Wright, T.J., Mansour, S.L., 2007. *Fgf3* is required for dorsal patterning and morphogenesis of the inner ear epithelium. Development 134, 3615–3625.
Hoffmann, A.D., Peterson, M.A., Friedland-Little, J.M., Anderson, S.A., Moskowitz, I.P., 2009. Sonic hedgehog is required in pulmonary endoderm for atrial septation. Development 136, 1761–1770.
Ilagan, R., Abu-Issa, R., Brown, D., Yang, Y.P., Jiao, K., Schwartz, R.J., Klingensmith, J., Meyers, E.N., 2006. *Fgf8* is required for anterior heart field development. Development 133, 2435–2445.
Itoh, N., Ornitz, D.M., 2008. Functional evolutionary history of the mouse *Fgf* gene family. Dev. Dyn. 237, 18–27.
Jia, Q., McDill, B.W., Li, S.Z., Deng, C., Chang, C.P., Chen, F., 2007. Smad signaling in the neural crest regulates cardiac outflow tract remodeling through cell autonomous and non-cell autonomous effects. Dev. Biol. 311, 172–184.
Kelly, R.G., Brown, N.A., Buckingham, M.E., 2001. The arterial pole of the mouse heart forms from *Fgf10*-expressing cells in pharyngeal mesoderm. Dev. Cell 1, 435–440.
Kirby, M.L., Hutson, M.R., 2010. Factors controlling cardiac neural crest cell migration. Cell Adh. Migr. 4 Epub ahead of print.
Kirby, M.L., Turnage III, K.L., Hays, B.M., 1985. Characterization of conotruncal malformations following ablation of "cardiac" neural crest. Anat. Rec. 213, 87–93.
Ko, S.O., Chung, I.H., Xu, X., Oka, S., Zhao, H., Cho, E.S., Deng, C., Chai, Y., 2007. *Smad4* is required to regulate the fate of cranial neural crest cells. Dev. Biol. 312, 435–447.
Ladher, R.K., Wright, T.J., Moon, A.M., Mansour, S.L., Schoenwolf, G.C., 2005. FGF8 initiates inner ear induction in chick and mouse. Genes Dev. 19, 603–613.
Lie-Venema, H., van den Akker, N.M., Bax, N.A., Winter, E.M., Maas, S., Kekarainen, T., Hoeben, R.C., deRuiter, M.C., Poelmann, R.E., Gittenberger-de Groot, A.C., 2007. Origin, fate, and function of epicardium-derived cells (EPDCs) in normal and abnormal cardiac development. ScientificWorldJournal 7, 1777–1798.
Lindsay, E.A., Vitelli, F., Su, H., Morishima, M., Huynh, T., Pramparo, T., Jurecic, V., Ogunrinu, G., Sutherland, H.F., Scambler, P.J., Bradley, A., Baldini, A., 2001. *Tbx1* haploinsufficiency in the DiGeorge syndrome region causes aortic arch defects in mice. Nature 410, 97–101.
Macatee, T.L., Hammond, B.P., Arenkiel, B.R., Francis, L., Frank, D.U., Moon, A.M., 2003. Ablation of specific expression domains reveals discrete functions of ectoderm- and endoderm-derived FGF8 during cardiovascular and pharyngeal development. Development 130, 6361–6374.
Männer, J., Pérez-Pomares, J.M., Macías, D., Muñoz-Chápuli, R., 2001. The origin, formation and developmental significance of the epicardium: a review. Cells Tissues Organs 169, 89–103.
Männer, J., Schlueter, J., Brand, T., 2005. Experimental analyses of the function of the proepicardium using a new microsurgical procedure to induce loss-of-proepicardial-function in chick embryos. Dev. Dyn. 233, 1454–1463.
Mansour, S.L., Goddard, J.M., Capecchi, M.R., 1993. Mice homozygous for a targeted disruption of the proto-oncogene *int-2* have developmental defects in the tail and inner ear. Development 117, 13–28.
Marguerie, A., Bajolle, F., Zaffran, S., Brown, N.A., Dickson, C., Buckingham, M.E., Kelly, R.G., 2006. Congenital heart defects in Fgfr2-IIIb and Fgf10 mutant mice. Cardiovasc. Res. 71, 50–60.
McCulley, D.J., Kang, J.O., Martin, J.F., Black, B.L., 2008. BMP4 is required in the anterior heart field and its derivatives for endocardial cushion remodeling, outflow tract septation, and semilunar valve development. Dev. Dyn. 237, 3200–3209.
Meyers, E.N., Martin, G.R., 1999. Differences in left–right axis pathways in mouse and chick: functions of FGF8 and SHH. Science 285, 403–406.
Min, H., Danilenko, D.M., Scully, S.A., Bolon, B., Ring, B.D., Tarpley, J.E., DeRose, M., Simonet, W.S., 1998. *Fgf-10* is required for both limb and lung development and exhibits striking functional similarity to *Drosophila branchless*. Genes Dev. 12, 3156–3161.
Mommersteeg, M.T., Dominguez, J.N., Wiese, C., Norden, J., de Gier-de Vries, C., Burch, J.B., Kispert, A., Brown, N.A., Moorman, A.F., Christoffels, V.M., 2010. The sinus venosus progenitors separate and diversify from the first and second heart fields early in development. Cardiovasc. Res. 87, 92–101.
Moon, A., 2008. Mouse models of congenital cardiovascular disease. Curr. Top. Dev. Biol. 84, 171–248.
Nie, X., Deng, C.X., Wang, Q., Jiao, K., 2008. Disruption of *Smad4* in neural crest cells leads to mid-gestation death with pharyngeal arch, craniofacial and cardiac defects. Dev. Biol. 316, 417–430.

Nomura-Kitabayashi, A., Phoon, C.K., Kishigami, S., Rosenthal, J., Yamauchi, Y., Abe, K., Yamamura, K., Samtani, R., Lo, C.W., Mishina, Y., 2009. Outflow tract cushions perform a critical valve-like function in the early embryonic heart requiring BMPRIA-mediated signaling in cardiac neural crest. Am. J. Physiol. Heart Circ. Physiol. 297, H1617–H1628.

Park, E.J., Ogden, L.A., Talbot, A., Evans, S., Cai, C.L., Black, B.L., Frank, D.U., Moon, A.M., 2006. Required, tissue-specific roles for Fgf8 in outflow tract formation and remodeling. Development 133, 2419–2433.

Park, E.J., Watanabe, Y., Smyth, G., Miyagawa-Tomita, S., Meyers, E., Klingensmith, J., Camenisch, T., Buckingham, M., Moon, A.M., 2008. An FGF autocrine loop initiated in second heart field mesoderm regulates morphogenesis at the arterial pole of the heart. Development 135, 3599–3610.

Pérez-Pomares, J.M., Phelps, A., Sedmerova, M., Carmona, R., González-Iriarte, M., Muñoz-Chápuli, R., Wessels, A., 2002. Experimental studies on the spatiotemporal expression of WT1 and RALDH2 in the embryonic avian heart: a model for the regulation of myocardial and valvuloseptal development by epicardially derived cells (EPDCs). Dev. Biol. 247, 307–326.

Pérez-Pomares, J.M., Phelps, A., Sedmerova, M., Wessels, A., 2003. Epicardial-like cells on the distal arterial end of the cardiac outflow tract do not derive from the proepicardium but are derivatives of the cephalic pericardium. Dev. Dyn. 227, 56–68.

Ponticos, M., 2010. The role of the homeodomain transcription factor Nkx2-5 in the cardiovascular system. In: Abraham, D., et al. (Ed.), Advances in Vascular Medicine. Springer, London, pp. 113–130.

Qi, X., Yang, G., Yang, L., Lan, Y., Weng, T., Wang, J., Wu, Z., Xu, J., Gao, X., Yang, X., 2007. Essential role of *Smad4* in maintaining cardiomyocyte proliferation during murine embryonic heart development. Dev. Biol. 311, 136–146.

Ratajska, A., Czarnowska, E., Ciszek, B., 2008. Embryonic development of the proepicardium and coronary vessels. Int. J. Dev. Biol. 52, 229–236.

Reese, D.E., Mikawa, T., Bader, D.M., 2002. Development of the coronary vessel system. Circ. Res. 91, 761–768.

Rochais, F., Mesbah, K., Kelly, R.G., 2009. Signaling pathways controlling second heart field development. Circ. Res. 104, 933–942.

Rohmann, E., Brunner, H.G., Kayserili, H., Uyguner, O., Nürnberg, G., Lew, E.D., Dobbie, A., Eswarakumar, V.P., Uzumcu, A., Ulubil-Emeroglu, M., Leroy, J.G., Li, Y., Becker, C., Lehnerdt, K., Cremers, C.W., Yüksel-Apak, M., Nürnberg, P., Kubisch, C., Schlessinger, J., van Bokhoven, H., Wollnik, B., 2006. Mutations in different components of FGF signaling in LADD syndrome. Nat. Genet. 38, 414–417.

Sekine, K., Ohuchi, H., Fujiwara, M., Yamasaki, M., Yoshizawa, T., Sato, T., Yagishita, N., Matsui, D., Koga, Y., Itoh, N., Kato, S., 1999. *Fgf10* is essential for limb and lung formation. Nat. Genet. 21, 138–141.

Snarr, B.S., O'Neal, J.L., Chintalapudi, M.R., Wirrig, E.E., Phelps, A.L., Kubalak, S.W., Wessels, A., 2007a. Isl1 expression at the venous pole identifies a novel role for the second heart field in cardiac development. Circ. Res. 101, 971–974.

Snarr, B.S., Wirrig, E.E., Phelps, A.L., Trusk, T.C., Wessels, A., 2007b. A spatiotemporal evaluation of the contribution of the dorsal mesenchymal protrusion to cardiac development. Dev. Dyn. 236, 1287–1294.

Snarr, B.S., Kern, C.B., Wessels, A., 2008. Origin and fate of cardiac mesenchyme. Dev. Dyn. 237, 2804–2819.

Snider, P., Olaopa, M., Firulli, A.B., Conway, S.J., 2007. Cardiovascular development and the colonizing cardiac neural crest lineage. ScientificWorldJournal 7, 1090–1113.

Song, L., Yan, W., Chen, X., Deng, C.X., Wang, Q., Jiao, K., 2007. Myocardial *Smad4* is essential for cardiogenesis in mouse embryos. Circ. Res. 101, 277–285.

Stottmann, R.W., Choi, M., Mishina, Y., Meyers, E.N., Klingensmith, J., 2004. BMP receptor IA is required in mammalian neural crest cells for development of the cardiac outflow tract and ventricular myocardium. Development 131, 2205–2218.

Tekin, M., Öztürkmen Akay, H., Fitoz, S., Birnbaum, S., Cengiz, F.B., Sennaroglu, L., Incesulu, A., Yüksel Konuk, E.B., Hasanefendioglu Bayrak, A., Sentürk, S., Cebeci, I., Ütine, G.E., Tunçbilek, E., Nance, W.E., Duman, D., 2008. Homozygous *FGF3* mutations result in congenital deafness with inner ear agenesis, microtia, and microdontia. Clin. Genet. 73, 554–565.

Torlopp, A., Schlueter, J., Brand, T., 2010. Role of fibroblast growth factor signaling during proepicardium formation in the chick embryo. Dev. Dyn. 239, 2393–2403.

Urness, L.D., Paxton, C.N., Wang, X., Schoenwolf, G.C., Mansour, S.L., 2010. FGF signaling regulates otic placode induction and refinement by controlling both ectodermal target genes and hindbrain *Wnt8a*. Dev. Biol. 340, 595–604.

van Wijk, B., van den Berg, G., Abu-Issa, R., Barnett, P., van der Velden, S., Schmidt, M., Ruijter, J.M., Kirby, M.L., Moorman, A.F., van den Hoff, M.J., 2009. Epicardium and myocardium separate from a common precursor pool by crosstalk between bone morphogenetic protein- and fibroblast growth factor-signaling pathways. Circ. Res. 105, 431–441.

Vincent, S.D., Buckingham, M.E., 2010. How to make a heart: the origin and regulation of cardiac progenitor cells. Curr. Top. Dev. Biol. 90, 1–41.

Vincentz, J.W., McWhirter, J.R., Murre, C., Baldini, A., Furuta, Y., 2005. *Fgf15* is required for proper morphogenesis of the mouse cardiac outflow tract. Genesis 41, 192–201.

Virágh, S., Challice, C.E., 1981. The origin of the epicardium and the embryonic myocardial circulation in the mouse. Anat. Rec. 201, 157–168.

Vitelli, F., Taddei, I., Morishima, M., Meyers, E.N., Lindsay, E.A., Baldini, A., 2002. A genetic link between *Tbx1* and fibroblast growth factor signaling. Development 129, 4605–4611.

Waldo, K.L., Kumiski, D., Kirby, M.L., 1996. Cardiac neural crest is essential for the persistence rather than the formation of an arch artery. Dev. Dyn. 205, 281–292.

Ward, C., Stadt, H., Hutson, M., Kirby, M.L., 2005. Ablation of the secondary heart field leads to tetralogy of Fallot and pulmonary atresia. Dev. Biol. 284, 72–83.

Watanabe, Y., Miyagawa-Tomita, S., Vincent, S.D., Kelly, R.G., Moon, A.M., Buckingham, M.E., 2010. Role of mesodermal FGF8 and FGF10 overlaps in the development of the arterial pole of the heart and pharyngeal arch arteries. Circ. Res. 106, 495–503.

Wright, T.J., Mansour, S.L., 2003. *Fgf3* and *Fgf10* are required for mouse otic placode induction. Development 130, 3379–3390.

Wright, T.J., Ladher, R., McWhirter, J., Murre, C., Schoenwolf, G.C., Mansour, S.L., 2004. Mouse FGF15 is the ortholog of human and chick FGF19, but is not uniquely required for otic induction. Dev. Biol. 269, 264–275.

Xu, C., Liguori, G., Persico, M.G., Adamson, E.D., 1999. Abrogation of the Cripto gene in mouse leads to failure of postgastrulation morphogenesis and lack of differentiation of cardiomyocytes. Development 126, 483–494.

Yang, L., Cai, C.L., Lin, L., Qyang, Y., Chung, C., Monteiro, R.M., Mummery, C.L., Fishman, G.I., Cogen, A., Evans, S., 2006. Isl1Cre reveals a common Bmp pathway in heart and limb development. Development 133, 1575–1585.

Zhang, J., Lin, Y., Zhang, Y., Lan, Y., Lin, C., Moon, A.M., Schwartz, R.J., Martin, J.F., Wang, F., 2008. *Frs2α*-deficiency in cardiac progenitors disrupts a subset of FGF signals required for outflow tract morphogenesis. Development 135, 3611–3622.

Zhou, W., Lin, L., Majumdar, A., Li, X., Zhang, X., Liu, W., Etheridge, L., Shi, Y., Martin, J., Van de Ven, W., Kaartinen, V., Wynshaw-Boris, A., McMahon, A.P., Rosenfeld, M.G., Evans, S.M., 2007. Modulation of morphogenesis by noncanonical Wnt signaling requires ATF/CREB family-mediated transcriptional activation of TGFbeta2. Nat. Genet. 39, 1225–1234.